REVIEWS OF MODERN PHYSICS VOLUME 41, NUMBER 4, PART I OCTOBER 1969

Nonforward Scattering of Hadrons and High-Energy Phenomenology*,†

CHARLES B. CHIU‡
Cavendish Laboratory, Cambridge, England

This review is divided into three parts. First, we survey the general features of nonforward scattering. We comment on two large-angle scattering models (the statistical model and the proposal for explaining the "breaks" in the differential cross section in terms of production cross sections) and discuss the axiomatic results on lower bounds and the asymptotic angular dependence. Second, we review the motivation and the general formalism of the multiple-scattering model and the qualitative success of the model—in particular, its application to the nonforward scattering. Third, we discuss the impact of the multiple-scattering model on high-energy phenomenology. Here, we emphasize that, in addition to providing a concrete model for large $|t|$ scattering, the multiple-scattering model contains virtues from both the optical model and the Regge-pole model. Similar to the absorption model, it helps to explain problems encountered in a pure Regge-pole model. On the other hand, it preserves the past success of the Regge-pole model and opens new possibilities for it.

CONTENTS

1. INTRODUCTION

At this stage there is no general theory available for describing high-energy hadron collisions over the entire angular range. For the convenience of discussion, we shall divide, in an approximate way, this entire range into three regions:

(A) The forward- and backward-peak regions.
(B) The intermediate momentum-transfer region.
(C) The large-angle region.

In region A, i.e., near the forward and backward direction, peripheral mechanisms generally dominate. At this stage, Regge-pole models seem to give an approximate description to the data, at least for inelastic and backward-elastic scattering. For forward-elastic scattering, the situation is more controversial; some authors prefer to have the exchange of the Pomeranchon trajectory with a relatively small slope to be the dominant contribution, while others prefer to introduce some non-Regge components (Chan, 1968). For scattering in the intermediate momentum-transfer region (region B), there has been considerable interest in describing the data by a multiple-scattering picture*: One describes scattering in this larger momentum-transfer region in terms of successive small momentum-transfer scatterings. So far, the multiple-scattering formalism used by various authors involves small-angle approximations, so this formalism is not suitable for describing

* Brief content of this paper was reported at the Rutherford Laboratory Theoretical Physics Meeting, December 1968.

† This research has been sponsored in part by the U.S. Air Force Office of Scientific Research, through the European Office of Aerospace Research, OAR, United States Air Force, under Grant AF EOAR 67-30.

‡ Present address: Department of Physics, California Institute of Technology, Pasadena, Calif.

* For examples, see Amati, Cini, and Stanghellini (1963), Contogouris (1966), Anselm and Dyatlov (1967a; 1967b; 1967c), Chou and Yang (1968a; 1968b), Durand and Lipes (1968), Chiu and Finkelstein (1968a; 1969), and Frautschi and Margolis (1968a; 1968b.)

large-angle scattering. We define region C to be the one where the present multiple-scattering formalism is not applicable. This region could start, for example, at $|t| \sim 2$–3 GeV^2 at some present energies, where t is the square of the four-momentum transfer. But in practice, some authors were obliged to push this boundary much further out in $|t|$. At this stage no comparable phenomenological model is available in the third region.

In this paper, we shall be concerned with the experimental features, phenomenological models, and theories available for scattering in regions B and C, or the nonforward scattering region, and with the connection between this nonforward region and the forward- and backward-peak region. We do not aim at a systematic coverage of all work available in connection with our proposed considerations. Instead, we will only review a few selected topics from our own point of view. The general content and the plane of this paper is as follows. In Sec. 2, we give a brief summary of the general features of the data in the nonforward scattering region. We comment on two specific models for large-angle scattering: the statistical model and the proposals for explaining the breaks in the differential cross section in terms of production cross sections; the axiomatic results in connection with lower bounds and the asymptotic angular dependence of the differential cross section. In Secs. 3 and 4, we review the motivation and the general formalism for multiple-scattering models. In Sec. 5, we survey the applications of various multiple-scattering models to scattering, especially in the intermediate momentum-transfer region (region B). We shall see that the multiple-scattering picture gives a reasonable description of the data. In view of this success, we study in Sec. 6 the multiple-scattering correction for those cases where the Regge-pole model gives an approximate description of the data, and comment on the impact of the multiple-scattering model on high-energy phenomenology as a whole. In Appendix A, we give some details of the axiomatic results mentioned previously. As an example of the multiple-scattering model, we include in Appendix B a specific multi-Pomeranchon exchange model constructed from the eikonal approximation.

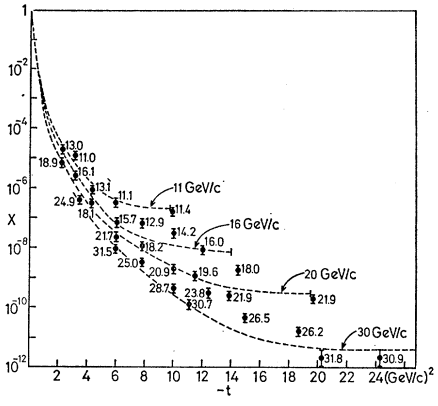

FIG. 1. The pp differential cross section versus t. The differential cross section is normalized to 1 at $t=0$. The dotted lines indicate the behavior of the angular dependence at several energies (from Cocconi *et al.*, 1965).

2. A SURVEY OF NONFORWARD SCATTERING

A. Early Large-Scale Data and on Statistical Model

The first extensive experiment on large-angle scattering was performed by the Brookhaven National Laboratory–Cornell group in 1963 on p–p scattering (Cocconi *et al.*, 1965). These results are illustrated in Fig. 1. Here the differential cross section is normalized to unity in the forward direction and plotted versus t. The dotted lines indicate the t dependence at different energies. These lines stop at 90°; for identical-particle scattering, the cross section is symmetric about 90°. Near the forward direction, the differential cross section is sharply peaked and is exponential in t or linear in the plot. As t increases, the differential cross section deviates from the exponential falloff and eventually flattens out towards 90°. At any fixed angle, the differential cross section falls off rapidly as a function of energy. These data are well described by an empirical expression, known as the Orear formula (Orear, 1964):

$$s(d\sigma/d\Omega) = a \exp(-p \sin\theta/b), \qquad (2.1)$$

where a and b are constants, p and θ are the momentum and the scattering angle of the proton in the c.m. system, respectively, and s the square of c.m. energy. For fixed angle, $s(d\sigma/d\Omega) \to \exp(-s^{1/2})$. This form is applicable away from the forward-peak region. At a fixed energy, when θ is small and yet finite, the differential cross section behaves like $\exp[-(-t)^{1/2}]$ as a function of t. In the large-angle region, especially toward 90°, $\sin\theta$ varies slowly. This results in the general flattening effect in the differential cross section. Because of the symmetry, the cross section must be flat at 90°. The np elastic differential cross section averaged over neutron laboratory momenta from 5.9 GeV/c to 7.2 GeV/c is illustrated in Fig. 2 (Allaby *et al.*, 1968a).* The pp cross section at 7 GeV/c is also included for comparison. Although from the symmetry argument the np cross section at 90° can have any slope, the data indicate that this is rather flat and is similar to the pp slope.

The fixed-angle energy dependence $\exp(-s^{1/2})$ and the flat distribution near 90° in the pp differential cross section was first explained in terms of the statistical model (Fast and Hagedorn, 1963; Fast, Hagedorn,

* The np data in Fig. 2 are from Kreisler *et al.* (1966). The dotted curve is from Manning *et al.* (1966). The pp data at 7 GeV/c is from Clyde (1966).

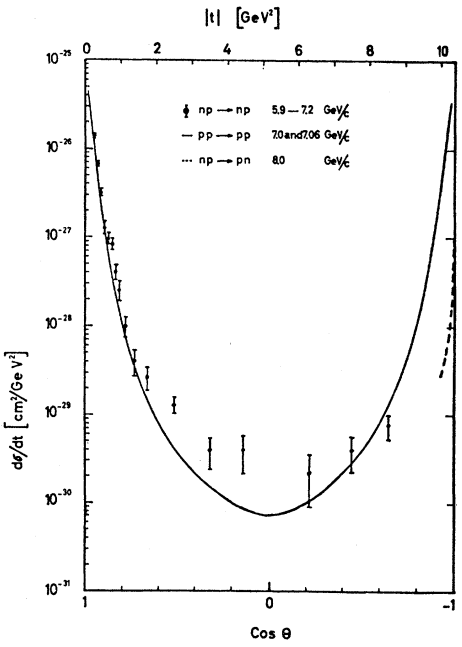

FIG. 2. The *np* differential cross section, averaged over neutron momenta between 5.9 and 7.2 GeV/*c*, compared to the *pp* cross section at 7 GeV/*c* from Allaby *et al.* (1968a). [The *np* data are from Kreisler *et al.* (1966). The dotted curve is from Manning *et al.* (1966).]

and Jones, 1963). In this model, when two protons collide, they form a compound system which then decays into any of the possible channels. The probability for decaying into any specific channel is directly proportional to the relevant phase space available. The higher the energy, the more channels opened. This in turn implies that there is less chance that the compound system will decay back into its original elastic channel. As a result, the *pp* differential cross section is expected to fall off rapidly as the energy increases. Detailed calculations indicate that the behavior exp $(-s^{1/2})$ is indeed what one expects from the consideration of phase space alone. Also, since phase space is all that has been considered, one expects the general flattening of the differential cross section in this large-angle region where the statistical model is applied. However, as was pointed out by Ericson (1966), if the large-angle scattering process is governed by the statistical mechanism, the phases and the magnitudes of the partial wave amplitudes are expected to be randomly distributed. This in turn will cause observable fluctuations in the differential cross section. In an experiment designed to look for such effects, no expected fluctuations were found (Allaby *et al.*, 1966). This strongly suggests that the large-angle scattering is not governed by some purely statistical process. Nevertheless, the phase space consideration mentioned above still remains an attractive interpretation for the exp $(-s^{1/2})$ energy dependence, especially near the 90° region.

B. Breaks in the *pp* Differential Cross Section

In 1967, a large body of the *pp* differential-cross-section data were summarized by Krisch (1967b)* on a plot of the differential cross section versus $\beta^2 p_\perp^2$; this is shown in Fig. 3. Very little theory has been advanced to explain the significance of this variable, $\beta^2 p_\perp^2 = tu/s$, where $u = 4m^2 - s - t$. Nevertheless, when the data are plotted in this variable, one sees that the experimental points, which are stretched out over 12 orders of magnitude, can be approximately represented by the sum of the three exponential functions. This indicates that the *pp* differential cross section at any fixed angle is divided into three energy regions, each of which has its own characteristic slope. It has been suggested that the three different slopes could be a reflection of the dominance of different types of inelastic processes. For example, Krisch (1967a) has associated these three regions with the effects due to the production of pions, kaons, and antinucleons, respectively. Allaby *et al.* (1967) and Kokkedee and Van Hove (1967) have suggested that the second break could be due to the onset of the baryon–antibaryon pair production, espe-

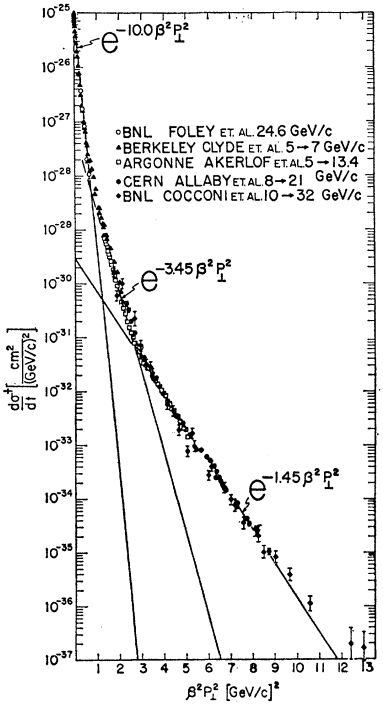

FIG. 3. The *pp* differential cross section plotted versus $\beta^2 p_\perp^2$. The lines indicate the three characteristic slopes in the differential-cross-section data (from Krisch, 1967b).

* We refer the reader to Krisch (1967b) for the details of the data. Also the $d\sigma^+/dt$ shown in Fig. 2 is not, strictly speaking, the differential cross section. It is the differential cross section multiplied by a monotonically decreasing factor, which equals 1 at $\theta = 0°$, and equals 0.5 at 90°.

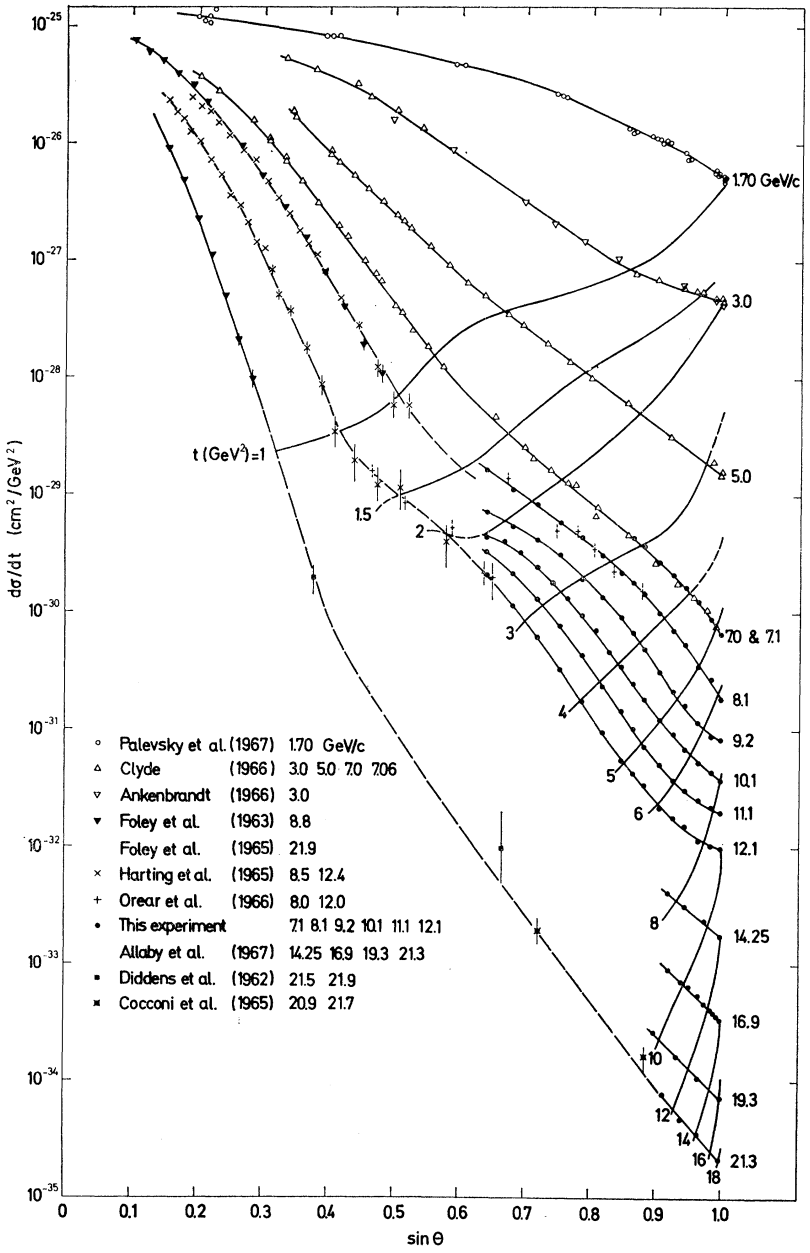

FIG. 4. The pp differential cross section in $d\sigma/dt$ plotted versus $\sin\theta$. Note the fine oscillatory pattern. The fixed t lines are included in the same plot (from Allaby *et al.*, 1968a).

cially near the 90° region. We shall see later in this section that the energy dependence of the position of the break could be in favor of this latter interpretation. These suggestions are attractive since, in an approximate manner, they correlate the positions of the breaks with the different production thresholds. To test these ideas more quantitatively, however, one requires some detailed knowledge of inelastic scattering. Krisch has formulated an ambitious phenomenological model and has explicitly taken into account all the inelastic production processes within it (Krisch, 1967a). Unfortunately, some simplifying assumptions of the model have recently been shown experimentally to be incorrect (Asbury *et al.*, 1968).* At this stage the correlation between simple features of inelastic scattering and the different slopes in the elastic differential cross section remains a conjecture.

In Fig. 4 the pp differential cross section is plotted as a function of $\sin\theta$. We see the oscillatory pattern, which is most complete at 12.1 GeV/c. There is a minimum in the slope between $|t|\approx 1$ and 2 GeV²

* In the Krisch model, the exponential dependence on $\beta^2 p_\perp^2$ of elastic scattering before the first break is assumed to be the same as that of $(d\sigma/dt)$ $(pp\to pp+\pi$'s) over the entire region of $\beta^2 p_\perp^2$ for pion production. The experiment showed that this assumption is incorrect.

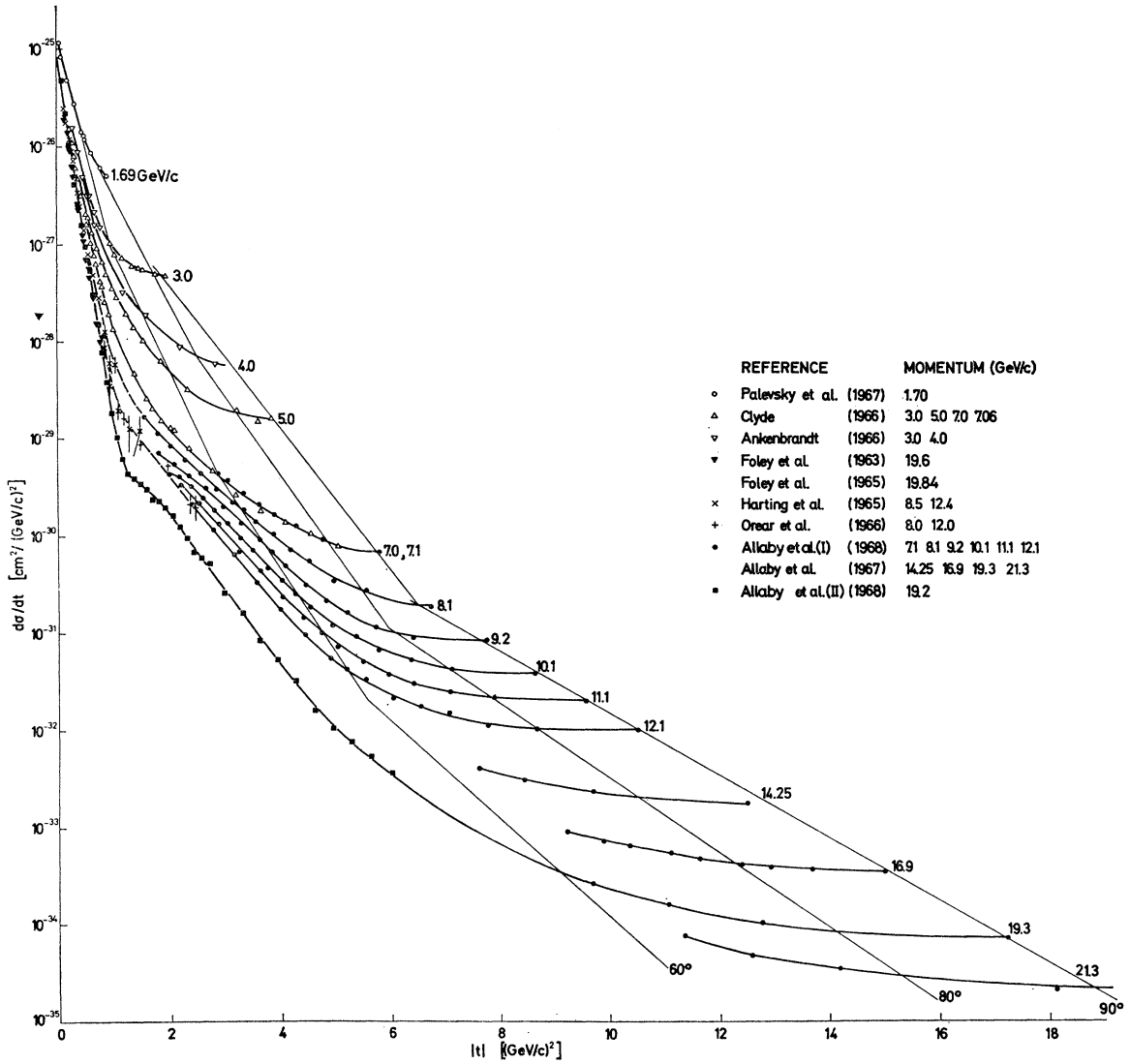

FIG. 5. The pp differential cross section in $d\sigma/dt$ plotted versus t. Note the movement of the break which occurs at $\sim$8.1 GeV/c at 90°; as the energy increases, the corresponding scattering angle decreases (from Allaby *et al.*, 1968b).

and another between $|t| \approx 6$ and 8 GeV^2. The dips here more or less correspond to the breaks in Krisch's plot. The angular distribution (Allaby *et al.*, 1968b) plotted versus t is shown in Fig. 5. This plot essentially summarizes the present status of pp scattering. It includes latest CERN data at $\sim$19.3 GeV/c, the highest energy at which the differential cross section has been measured over the entire angular region. The exp (t) behavior near the forward direction, the exp $[-(-t)^{1/2}]$ behavior in the intermediate momentum-transfer region, and the general flattening of the differential cross section in the large-angle region are well mapped out by the data. The exp $[-(-t)^{1/2}]$ behavior is more clearly illustrated in Fig. 6. Beyond $\theta \approx 60°$, the data deviate away from this behavior. The fixed-angle energy dependence of the cross section is given in Fig. 5. Along the 90° line, the break occurs at $\sim$8 GeV/c, and it moves to higher energies as the angle decreases. At 80°, it is at $P_L \sim 9$ GeV/c, and at 60°, at $P_L \sim 12$ GeV/c. As mentioned in the beginning of this section, Allaby *et al.* (1967) and Kokkedee and Van Hove (1967) have associated this break with the effect of baryon–antibaryon pair production. They observed that the production threshold is relatively close to the position of the break and argued that this production must affect first the s-wave elastic amplitude and, as energy increases, the higher partial waves are affected as well. Consequently, one expects the break to move to higher energies as the angle decreases; this qualitative statement is in agreement with the data. However, detailed calculations must be made in order to make it convincing.

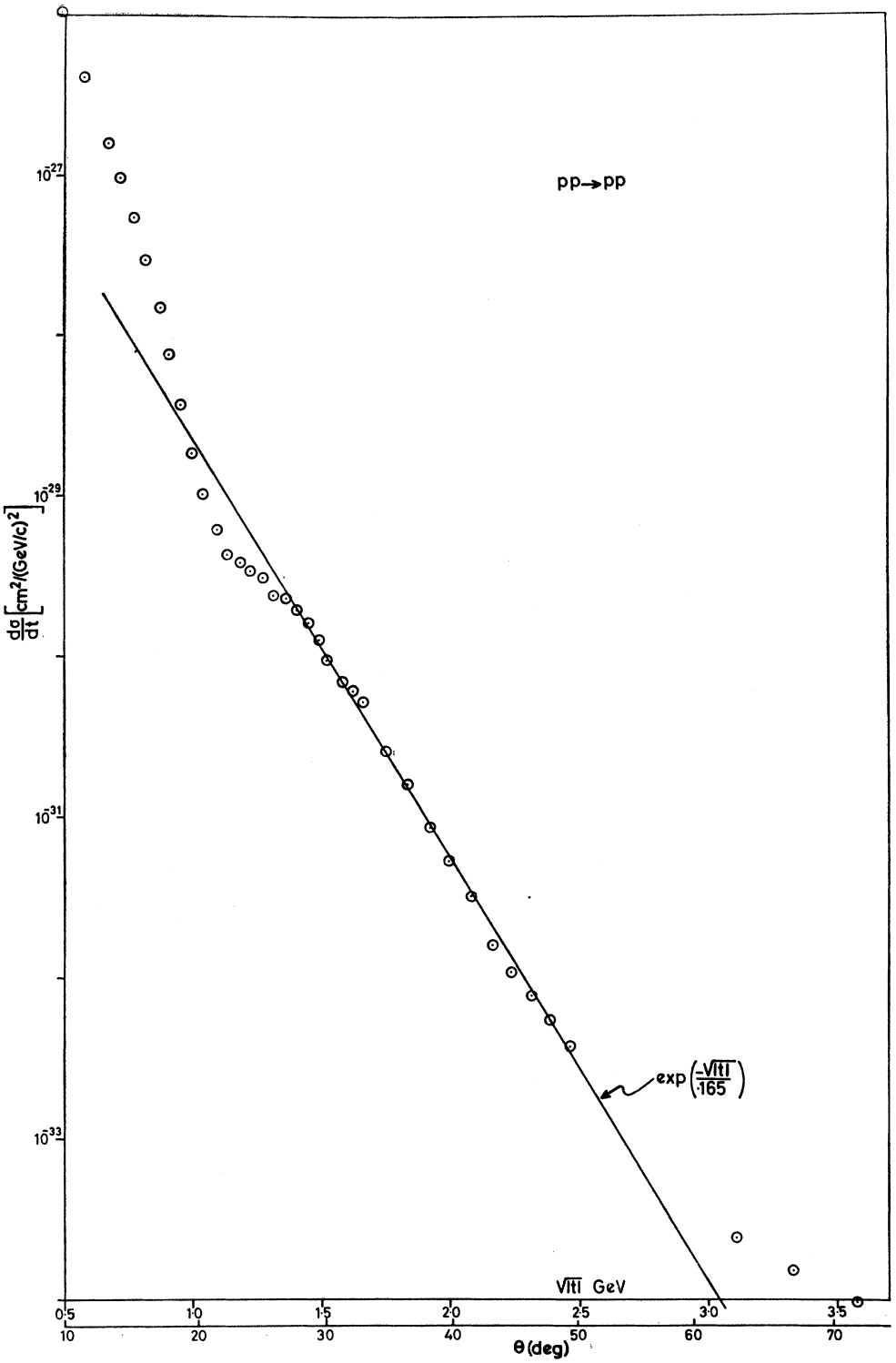

FIG. 6. The pp differential cross section plotted versus $(-t)^{1/2}$ at $\sim$ 19.2 GeV/c. The t dependence of the cross section in the intermediate momentum transfer is given by $\sim\exp[-(-t)^{1/2}/0.160]$. Data points are from Allaby *et al.* (1968b).

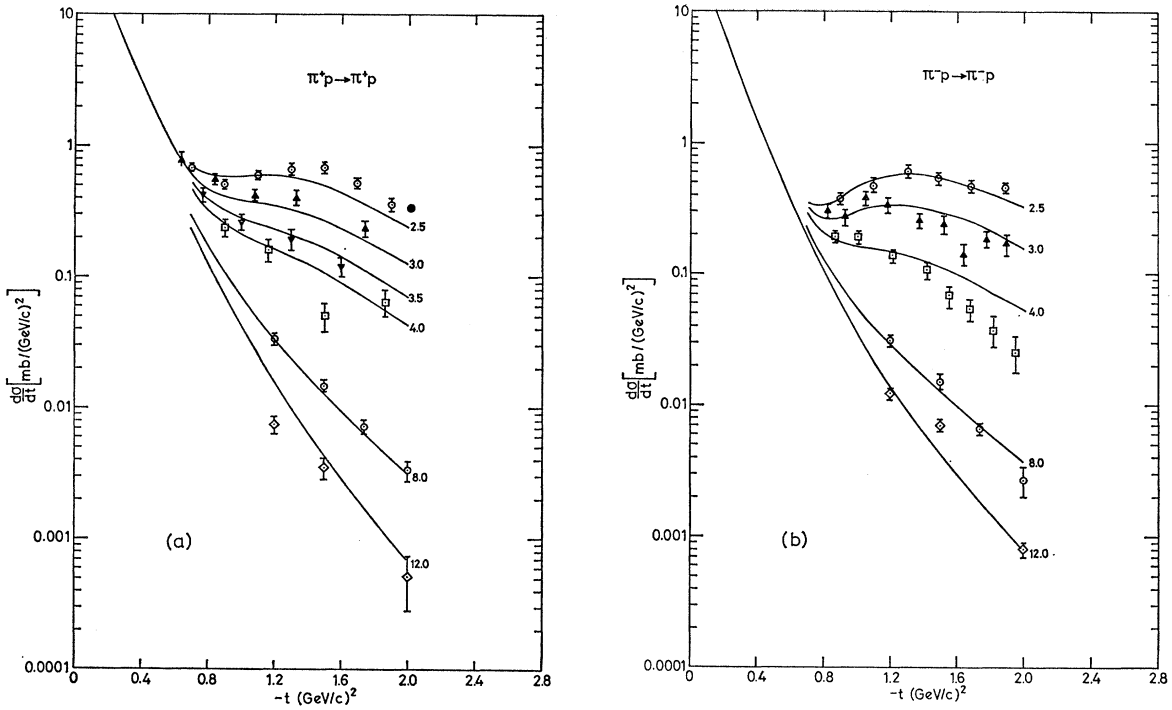

FIG. 7. The $\pi^{\pm}p$ differential cross sections versus t, by Chiu, Chu, and Wang (1967). The data points are from Coffin *et al.* (1966; 1965), Foley *et al.* (1963a), and Orear *et al.* (1966).

C. The $\pi^{\pm}\bar{p}$, $p^{-}p$, and $K^{-}p$ Differential Cross Section

The $\pi^{\pm}p$ differential cross section from $t=0$ to $t=-2$ GeV² is illustrated in Fig. 7.* The general features of the $\pi^{+}p$ and the $\pi^{-}p$ cross sections in this momentum-transfer interval are similar. Their forward peaks have a weak energy dependence. This peak extends to around $|t| = 0.8$ GeV². In the low-energy region, the cross section has a minimum here. As $|t|$ further increases, this minimum is followed by a secondary maximum. This secondary maximum has a strong energy dependence. The $\pi^{-}p$ data by the Cornell–BNL collaboration are illustrated in Fig. 8 (Bellettini, 1968; Ashmore, 1968; Orear, 1968a). Here the data are extended to $|t| \approx 6$ GeV² for the laboratory momenta from 5.8–13.6 GeV/c. More structure is found in the large-momentum-transfer region; note in particular the pronounced dip near $|t| = 3$ GeV².

The $\pi^{\pm}p$ data shown in Fig. 7 were analyzed in terms of the Regge-pole model by Chiu, Chu, and Wang (1967); those curves illustrated are their fits to the data. Here they assume that the secondary maximum is mainly due to the contribution of the P' trajectory, where $\alpha_{P'} \approx -0.5$ to -1. The energy dependence of the cross section when dominated by one Regge pole is given by $d\sigma/dt \sim s^{2\alpha-2}$. As energy increases, this secondary maximum falls off rapidly. Barger and Phillips (1968; 1969) and also Booth (1968) and Beretvas and Booth (1969) have associated dips in the $\pi^{-}p$ cross section (e.g., at $|t| \approx 3$ GeV²) and those in the $K^{-}p$ and $\bar{p}p$ differential cross sections (which we shall come to later on) with some speculated zeros in the Regge-pole residue functions. Barger and Phillips (1968) also have produced impressive fits to

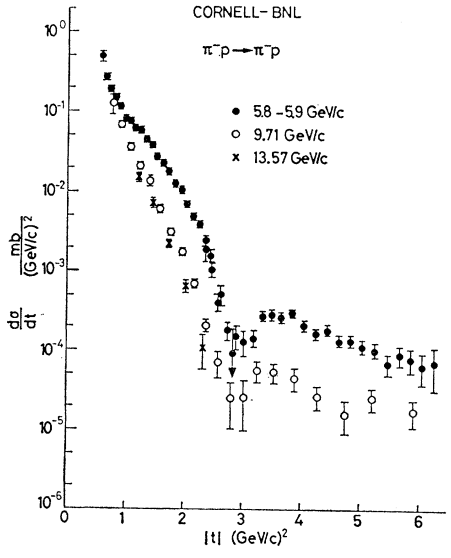

FIG. 8. Differential cross section for $\pi^{-}p$ scattering between ~6 and ~13.5 GeV/c incident laboratory momentum (from Bellettini, 1968; Ashmore *et al.*, 1968; Orear *et al.*, 1968a).

* Data points are from Coffin *et al.* (1966; 1965), Foley *et al.* (1963a), and Orear (1966).

the $\pi^- p$ differential cross section data from $p_{\text{Lab}}=3.5$ GeV/c to 13 GeV/c for $|t| \lesssim 4$ GeV^2, and the $\pi^\pm p$ polarization at 5.15 GeV/c for $|t| \lesssim 2$ GeV^2. In these fits, the Regge-pole residue functions having these speculated zeros incorporated are left to be freely adjusted and several pole terms are used to fit the data. At this stage, it is not clear whether their fits should be regarded as evidence for the dominance of the Regge-pole contributions in the large $|t|$ region. In fact, within the multiple-scattering model, for large $|t|$, the amplitude is dominated by the exchange of multi-Reggeons or Regge cuts, but not the Regge-pole terms.

The $\bar{p}p$ differential-cross-section data* are illustrated in Fig. 9. The curves shown in the same figure are the pp cross sections at comparable energies. They are included for comparison. The $\bar{p}p$ forward peak is sharper than the pp peak. As energy increases the $\bar{p}p$ peak expands while the pp peak shrinks. The $\bar{p}p$ differential cross section appears to have more structure than the pp cross section. In the $\bar{p}p$ cross section, there is a dip near $|t|=0.5$ GeV^2; there is another suppression in the differential cross section near $|t|=1.8$ GeV^2. Note in particular the oscillatory pattern in the data.

The $K^- p$ differential cross section† is shown in Fig. 10. The full line represents the data at 10 GeV/c multiplied by a factor of 100. From the comparison between this line and the forward peak at 5.5 GeV/c, indicated by the data, one sees that the $K^- p$ forward

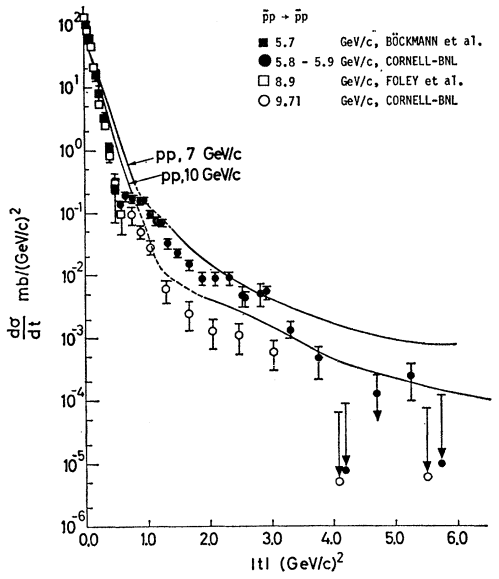

FIG. 9. Differential cross section for $\bar{p}p$ elastic scattering at ~5.8 and 9.7 GeV/c. The pp cross sections at ~7 and ~10 GeV/c indicated by the curves are included for comparison (from Bellettini, 1968; Ashmore *et al.*, 1968; Orear *et al.*, 1968a; Böckmann *et al.*, 1966; Foley *et al.*, 1963b).

* The $\bar{p}p$ data: Cornell–BNL collaboration (see Ashmore *et al.*, 1968; Orear *et al.*, 1968a; Böckmann *et al.*, 1966; Foley *et al.*, 1963b).

† The $K^- p$ data. Cornell–BNL collaboration (see Ashmore *et al.*, 1968; Orear *et al.*, 1968a); Mott *et al.*, 1966.

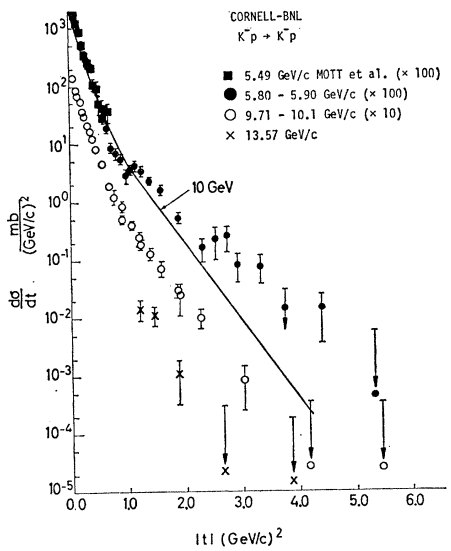

FIG. 10. Differential cross section for $K^- p$ scattering. The full line shows the qualitative behavior of the 10-GeV/c data after multiplying by a factor of 100 (from Bellettini, 1968; Ashmore *et al.*, 1968; Orear *et al.*, 1968a; Mott *et al.*, 1966).

peak expands somewhat as the energy increases, similar to the $\bar{p}p$ peak. At 5.5 GeV/c, there is a dip in the cross section near $|t|=1.0$ GeV^2 and another possible one at 2 GeV^2. There is a significant oscillatory pattern in the cross section, although at 10 GeV/c this pattern appears to be much less pronounced.

To sum up, we see that the oscillatory pattern in the differential cross section is present one way or another in all the cross-section data that we have looked at. For some processes these patterns are pronounced, whereas for others, less so. These patterns also vary as a function of energy. We shall see later that in a diffraction or multiple-scattering model, it is natural to expect an oscillatory pattern in the differential cross section which could, in general, vary as a function of energy. This suggests that these models could be of relevance in describing hadron collisions at high energies. We also have mentioned the qualitative behavior of the forward peak for the various processes. We have mentioned its t dependence, the sharpness of the peak, and its s dependence, which is the shrinkage property of the peak. We shall see that the diffraction model and multiple-scattering model also provide some qualitative statements on these features.

D. The Generalized Cerulus–Martin Fixed-Angle Lower Bound and the Tiktopoulos–Treiman Angular Dependence

We comment on some formal results obtained from an axiomatic approach here. In Fig. 3, if the differential cross section after the second break persists in behaving like $\exp(-\beta^2 p_\perp^2)$, then

$$\frac{d\sigma}{dt} \xrightarrow[s\to\infty]{\text{fixed } \theta} \exp(-s). \tag{2.2}$$

This violates the Cerulus–Martin fixed-angle lower bound (Cerulus and Martin, 1964) which states that at any fixed angle the scattering amplitude cannot fall off asymptotically faster than $\exp(-s^{1/2}\ln s)$. However, it was pointed out by Tan and the author (Chiu and Tan, 1967), by Eden and Tan (1968), and also emphasized recently by Epstein (1968) that this bound is sensitive to the domain of the polynomial boundedness assumed in the original derivation. If one alters this domain, one can obtain different lower bounds. For example, for the domain corresponding to a linearly rising Regge trajectory, the bound becomes $\exp(-s\ln s)$, and the behavior $\exp(-\beta^2 p_\perp^2)$ in the differential cross section will not violate this bound. We refer the reader to Appendix A for further details.

Although the variable $\beta^2 p_\perp^2$ has not been motivated at this stage, Tiktopoulos and Treiman (1968) have recently given a special meaning to the angular dependence $\sin\theta$ occurring in the exponential function of the Orear formula [cf. Eq. (2.1)]. With certain axiomatic assumptions, they show that the $\sin\theta$ dependence necessarily follows. We again refer the reader to Appendix A for further details. The experimental data (Allaby *et al.*, 1968a) plotted against $p\sin\theta$ are shown in Fig. 11. The dotted line is the Orear fit. The average behavior of all the points beyond $p\sin\theta=1$ GeV/c is well described by the fit, although there is some systematic deviation at smaller values of $p\sin\theta$. The over-all fit to the data is reasonable; this suggests that the axiomatic assumptions of Tiktopoulos and Treiman could be reasonable. We remark here that for both the fixed-angle lower bound and the asymptotic angular dependence discussed here, one is concerned with the asymptotic behavior of the amplitude. If in the future the differential cross section continues to show breaks at the higher-energy regions, these comparisons might not be relevant.

3. THE OPTICAL MODEL, EIKONAL APPROXIMATION, AND THE MULTIPLE-SCATTERING MODEL

A. The Impact-Parameter Representation

We first discuss the impact-parameter representation. This representation is particularly appropriate for describing high-energy, small-angle scattering, where there are many partial waves contributing and the phase shifts vary smoothly as a function of l.

Consider a scattering amplitude f, for simplicity with equal mass and spinless external particles. The partial wave expansion is defined as

$$f=(1/2ip)\sum_l (2l+1)P_l(z)[\exp(2i\delta_l)-1] \quad (3.1)$$

and

$$d\sigma/d\Omega=|f|^2. \quad (3.2)$$

For high-energy, small-angle scattering, where $(1-z)$ is small, one makes the following replacements:

$$(l+\tfrac{1}{2})\to bp,$$
$$2\delta_l\to\chi(b),$$
$$P_l(z)\to J_0(xb) \quad \text{with} \quad x=(-t)^{1/2},$$

and

$$\sum_l \to p\int_0^\infty db. \quad (3.3)$$

Here b and $\chi(b)$ are the impact parameter and the phase-shift function (or the eikonal function), respectively. Thus

$$f(s,t)=ip\int_0^\infty J_0(xb)\{1-\exp[i\chi(b)]\}b\,db \equiv ip\langle 1-\exp(i\chi)\rangle, \quad (3.4)$$

$$\exp[i\chi(b)]-1=\frac{i}{p}\int_0^\infty x\,dx J_0(xb)f(s,-x^2)\equiv\frac{i}{p}\langle f\rangle. \quad (3.5)$$

The symbol $\langle\ \rangle$ denotes the Fourier–Bessel transform. To proceed further, one has to make specific assumptions about $\chi(b)$, the phase shift. Let us first see how $\chi(b)$ is motivated in an optical model.

B. The Optical Model and the Chou–Yang Model

We follow the notation of Chou and Yang (1968a) here. Consider a plane wave passing through an absorptive slab with thickness d. The transmission coefficient of the slab is given by

$$S(b)\equiv\exp[i\chi(b)]=\exp[-\alpha(b)d]. \quad (3.6)$$

Here the total phase shift $\chi(b)$ is proportional to the term $-\ln S=\alpha d$, which is referred to as the opaqueness of the slab. Similarly, for the scattering of waves by a spherically symmetric object, one can also define the quantity opaqueness, $-\ln S$, at any impact parameter b. Motivated by this picture of classical optics, hadrons are described in a diffraction or optical model as objects with an extended structure characterized by some spherically symmetric "opaqueness density" $\rho(x, y, z)$, which is related to the Fourier–Bessel transform of the hadronic form factor. Let us consider the collision of two hadrons A and B moving parallel to the z axis. To each point in A, B appears to be a disc with the opaqueness density ρ being integrated along the z direction, and vice versa for each point in B. For the collision one assumes that the phase shift is proportional to the total amount of matter overlapped. In small-angle approximation it can be shown that this overlapped amount is given by the Fourier–Bessel transform of the products of the form factors for these two hadrons; in other words,

$$i\chi\propto\langle F_A(t)F_B(t)\rangle. \quad (3.7)$$

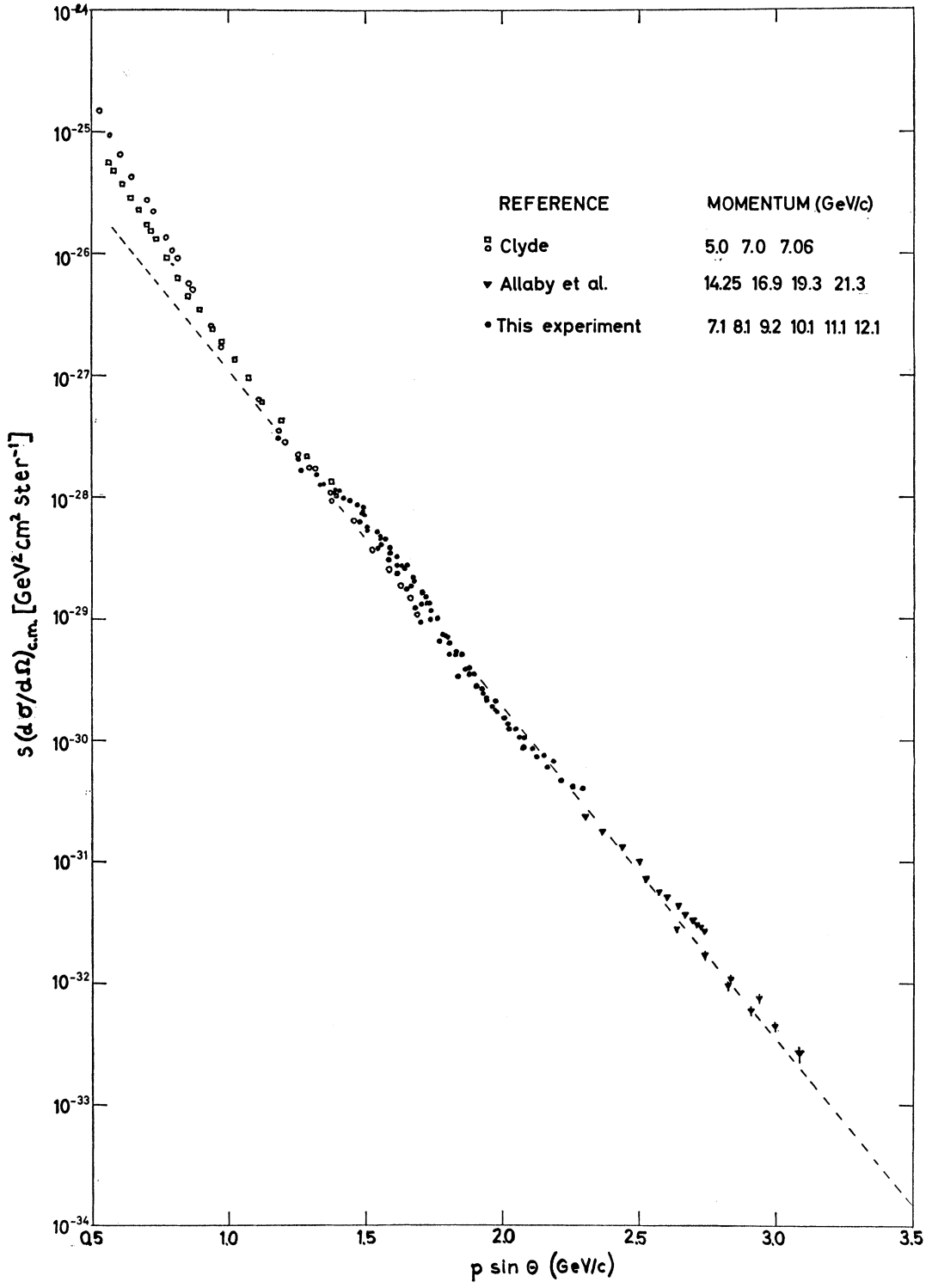

FIG. 11. The pp differential cross section in $s(d\sigma/d\Omega)$ plotted versus $p \sin\theta$. The dotted line indicates the Orear fit (from Allaby *et al.*, 1968a).

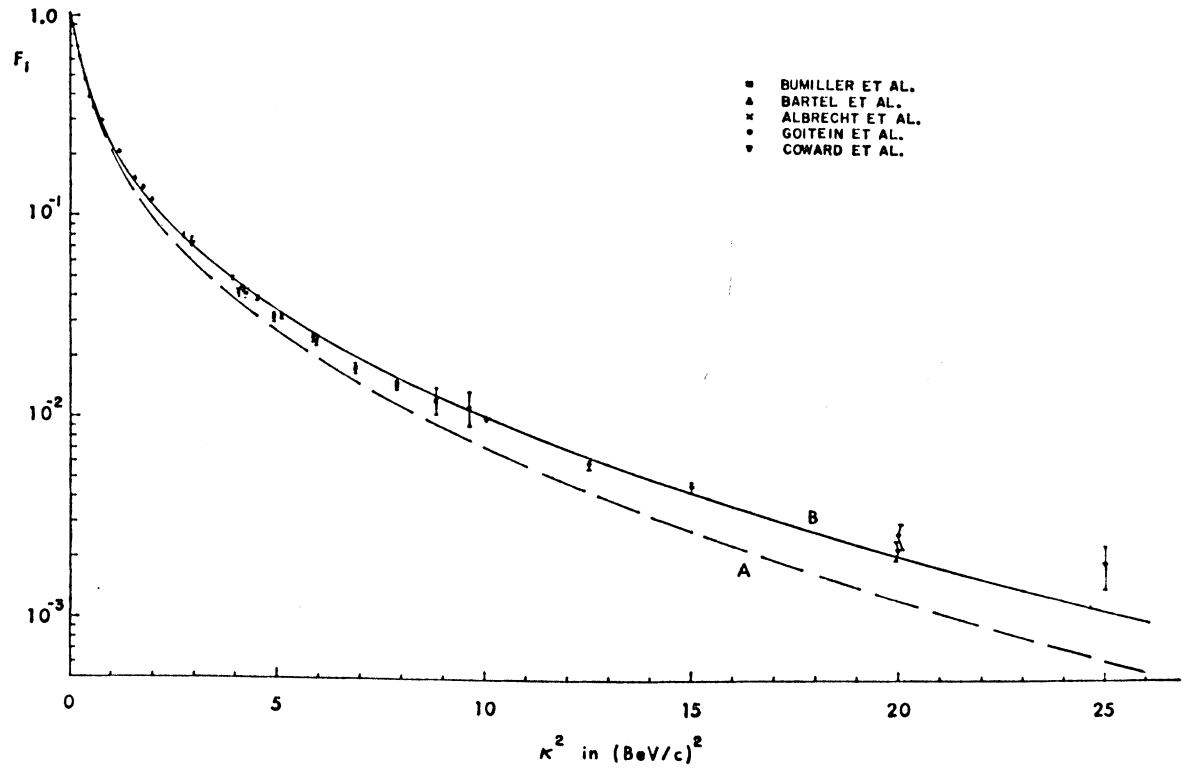

FIG. 12. The comparison between the calculated matter form factor (curves A and B) and the electric-charge-form-factor data (from Chou and Yang, 1968a).

Historically, the correlation between the collision amplitude and the proton form factor was first suggested by Wu and Yang (1965). They proposed that the pp scattering differential cross section at large momentum transfer should be proportional to the fourth power of the proton charge form factor. Later on, the same relation was noted by several authors (for example, Van Hove, 1966) to be approximately valid in the small $|t|$ region. In the droplet model, Byers and Yang (1966) developed the above diffraction picture in connection with small-angle inelastic scattering. The specific prescription of Eq. (3.7) was suggested by Chous and Yang (1968a; 1968b). They write for pp scattering

$$i\chi(b) = -c\langle F_p^2 \rangle. \tag{3.7a}$$

Here c is some constant which is taken to be independent of energy. So their amplitude f as defined by Eqs. (3.4) and (3.7a) is an asymptotic amplitude. Here χ is real, which corresponds to the phase shift induced by a purely absorptive medium.

If the matter form factor is given, for a specific value of c one can proceed to calculate the asymptotic scattering amplitude f from Eqs. (3.7a) and (3.4). Alternatively, if one makes some conjecture about the asymptotic pp scattering amplitude through Eq. (3.5) and the relation

$$|F_p(t)|^2 \propto \langle i\chi \rangle, \tag{3.8}$$

one can calculate the matter form factor of the proton, F_p.

Chou and Yang assumed that the asymptotic pp differential cross section near the forward direction can be approximated by the present pp data at the highest available energy. They gave two possibilities:

$$\text{(A)}\quad d\sigma/dt = \text{const}\exp(10.3t),$$

$$\text{(B)}\quad d\sigma/dt = \text{const}[\exp(5.5t) + 0.015\exp(2t)]^2. \tag{3.9}$$

The matter form factors were then calculated from Eqs. (3.9), (3.5), and (3.8). The results are shown in Fig. 12 as curves A and B. The data points correspond to the electric charge form factor of the proton. It is surprising to see that the curve of the matter form factor is practically in coincidence with the charge-form-factor data. This means that the matter distribution and the charge distribution in a proton are extremely similar. If one takes this coincidence seriously, it seems to suggest that this is indeed an asymptotic limit for the scattering amplitude. Also, the near forward differential cross section, as given by Eq. (3.9), is in fact close to the asymptotic amplitude. It turns out that this coincidence is not sensitive to the differential cross section at large $|t|$, so that no statement can be made about the asymptotic behavior of the pp

differential cross section in the large $|t|$ region at this point.

Chou and Yang (1968b) and also Durand and Lipes (1968) have calculated the pp differential cross section from the form-factor data and the adjustable parameter c. They found that the calculated pp differential cross section in the nonforward region is particularly sensitive to the detailed t dependence of the matter form factor and the value of c assumed. However, over a wide range of the possible values for the form factor $F_p(t)$ and the parameter c, oscillations were persistently found in the calculated cross section. This led Durand and Lipes to predict the existence of the diffraction pattern in the asymptotic cross section. Among various possibilities, two of their calculated cross sections are shown in Fig. 13. Curve a is the asymptotic differential cross section with a real value of c, and curve b is obtained by using a complex value for c. The asymptotic cross section displays two diffraction zeros. These zeros are partly filled in when the real part of the amplitude is included as indicated by b. They also investigated some possible spin-dependent effects by fitting the near forward pp polarization data at 6–12 GeV/c. They found that, due to the presence of the first diffraction zero in the asymptotic cross section, the pp polarization has a minimum near $|t| \approx 1$–2 GeV^2. Apparently this feature is seen in the recent polarization data by the Chicago–Argonne group at 5 GeV/c (Bellettini, 1968).

Finally, although the structure shown in Fig. 13 is quite reminiscent of the pp differential cross section discussed in Sec. 2, the asymptotic cross section, especially in the large $|t|$ region, is far from the experimental data. To describe the large momentum-transfer differential cross section, one must incorporate energy dependence into $f(s, t)$. We shall proceed first to discuss

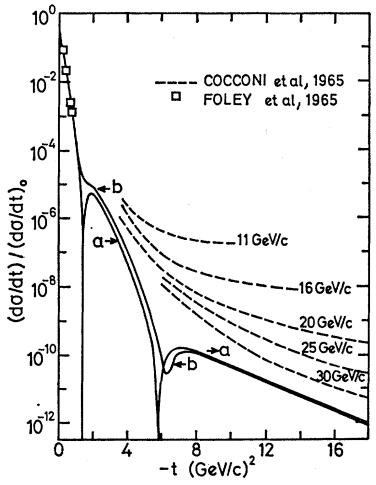

FIG. 13. The pp asymptotic differential cross section (curves a and b) predicted from the Chou–Yang model as calculated by Durand and Lipes. The dotted lines indicate the behavior of the data at present experimental energies, for purposes of comparison (from Durand and Lipes, 1968).

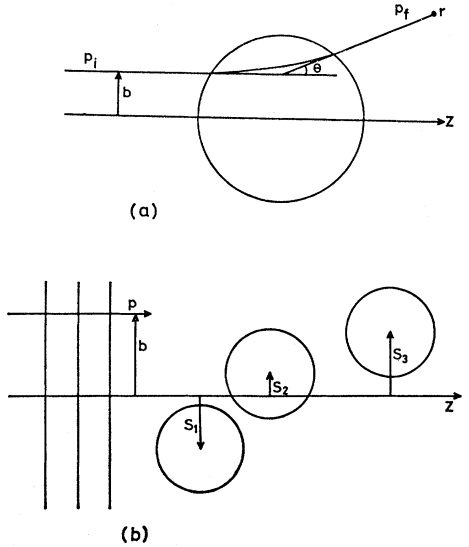

FIG. 14. (a) The trajectory for a scattered ray at an impact parameter b. (b) The incident wave and the scattering centers.

the eikonal approximation and topics related to multiple scattering and defer the discussion for incorporating the energy dependence in the Chou–Yang model to Sec. 5 and Sec. 6.

C. Eikonal Approximation and the Multiple-Scattering Model

First we investigate how the interaction potential is related to the phase shift through the eikonal approximation.* Consider the scattering of a particle with mass $m=\frac{1}{2}$ and momentum p from a potential V. Here the Schrödinger equation is given by

$$\nabla^2\psi+[p^2-V(r)]\psi=0. \tag{3.10}$$

We assume the potential $V \ll p^2$. Let the initial momentum $\mathbf{p}_i$ be parallel to the z direction at impact parameter b [see Fig. 14(a)]. Using the WKB approximation, one finds the wave function at a point $\mathbf{r}$ near the forward direction given by Glauber (1959; 1967):

$$\psi \approx \exp\left[i\mathbf{p}\cdot\mathbf{r}+i\int_{-\infty}^{z} dz'\,(\{p^2-V[(z'^2+b^2)^{1/2}]\}^{1/2}-\mathbf{p})\right]$$

$$\approx \exp\left\{i\mathbf{p}_i\cdot\mathbf{r}-\frac{i}{2p}\int_{-\infty}^{z} dz' V[(z'^2+b^2)^{1/2}]\right\}. \tag{3.10a}$$

We are interested in the amplitude for the scattering from the initial momentum $\mathbf{p}_i$ to the final momentum $\mathbf{p}_f$ [see Fig. 14(a)]. From quantum mechanics this amplitude is given by

$$f(\mathbf{p}_i\to\mathbf{p}_f)=-\frac{1}{4\pi}\int d^3r \exp(-i\mathbf{p}_f\cdot\mathbf{r})\,V(r)\psi(\mathbf{r}). \tag{3.11}$$

* Here we follow the notation of Wilkin (1967) and Glauber (1959).

Combining Eqs. (3.10a) and (3.11), after some algebra one obtains

$$f=-\frac{ip}{2\pi}\int d^2b\,\exp(i\mathbf{q}\cdot\mathbf{b})\{\exp[i\chi(b)]-1\} \quad (3.12)$$

$$=-ip\int_0^\infty J_0(|\mathbf{q}|b)\{\exp[i\chi(b)]-1\}bdb, \quad (3.13)$$

where

$$\chi(b)=-\frac{1}{2p}\int_{-\infty}^{\infty}dzV[(z^2+b^2)^{1/2}]$$

and

$$\mathbf{q}=\mathbf{p}_f-\mathbf{p}_i, \qquad |\mathbf{q}|=2p\sin(\theta/2).$$

We see Eq. (3.12) is precisely the same as the impact-parameter representation for an amplitude [see Eq. (3.4)]. Thus we refer to Eq. (3.13) as the phase-shift function for the potential V in the eikonal approximation. The function $\chi(b)$ is the corresponding eikonal function for V.

If there is more than one potential present, such as in Fig. 14(b),

$$V(b)=V_1(b-s_1)+V_2(b-s_2)+V_3(b-s_3)+\cdots, \quad (3.14)$$

and one finds

$$\chi(b)=\chi_1(b-s_1)+\chi_2(b-s_2)+\chi_3(b-s_3)+\cdots, \quad (3.15)$$

where the resultant phase shift is given by the sum over the phase shifts due to the individual potentials. Expressions identical to Eq. (3.15) can also be obtained for the relativistic wave equations.

Now let us comment briefly on the multiple-scattering picture in Glauber theory (Glauber, 1959; 1967). We consider the example of high-energy, small-angle nucleon–nucleus scattering. Here each nucleon in the nucleus is treated as a scattering center. The phase shift due to the collision between the incident nucleon and the individual nucleon in the nucleus is assumed to be known. The resultant phase shift for the nucleon–nucleus scattering is obtained by summing over all the phase shifts due to the interaction between the incident nucleon and each nucleon in the nucleus, as prescribed by Eq. (3.15). Note this additivity of phase shifts is the basic assumption in the Glauber theory. Although this expression of Eq. (3.15) was originally motivated by potential scattering, it is postulated that this expression is valid in general in the small-angle, high-energy approximation, even if the potential is not defined.

Glauber showed that if one assumes the energies transferred during the collision are negligibly small and the initial nucleon velocities do not alter the basic interactions, the amplitude for collisions in which the nucleus goes from an initial state $|i\rangle$ to a final state $|f\rangle$ is given by

$$F_{fi}=\frac{ip}{2\pi}\int\exp[i(\mathbf{p}_f-\mathbf{p}_i)\cdot\mathbf{b}]\langle f|\,\Gamma(b,s_1\cdots s_A)\,|i\rangle d^2b, \quad (3.16)$$

where there are A nucleons in the nucleus, and

$$\Gamma(b,s_1\cdots s_A)=1-\exp[i\chi(b,s_1\cdots s_A)]$$
$$=1-\exp[\chi_1(b-s_1)+\chi_2(b-s_2)+\cdots+\chi_A(b-s_A)]. \quad (3.16a)$$

The initial momentum is $\mathbf{p}_i$ and the final momentum $\mathbf{p}_f$, with $|\mathbf{p}_i|=|\mathbf{p}_f|=p$. To evaluate F_{fi} one must specify the structure of the initial and final wave functions. We will not go into this here. However, it is interesting to look at the structure of Γ. From Eq. (3.15)

$$\Gamma(b,s_1\cdots s_A)=1-\prod_{j=1}^{A}\{1-\Gamma_j(b-s_j)\}$$
$$=\sum_j\Gamma_j(b-s_j)-\sum_{j<m}\Gamma_j(b-s_j)\Gamma_m(b-s_m)$$
$$\sum\Gamma\Gamma\Gamma+\cdots. \quad (3.17)$$

Terms on the right-hand side of Eq. (3.17) correspond to single-, double-, triple-, ···, scattering terms between the incident nucleon and the nucleons in the target nucleus. This is a multiple-scattering series. Due to the small-angle approximation in Eq. (3.17), the same nucleon index never occurs twice in any given term and one never has more than A-fold scattering.

Now we come back to the nucleon–nucleon scattering. Let us start with the impact-parameter representation for the amplitude and assume that the eikonal function is given. We expand the factor $(e^{i\chi}-1)$ in Eq. (3.12) and obtain

$$e^{i\chi}-1=i\chi+\frac{(i\chi)^2}{2!}+\frac{(i\chi)^3}{3!}+\cdots. \quad (3.18)$$

In discussing nucleon–nucleon scattering or, in general, two-body hadron collisions, some authors find* that it is convenient to borrow the terminology used for the Glauber series of Eq. (3.17) by formally referring to the term linear in χ as the "single-scattering term" for nucleon–nucleon scattering, in analogy to referring to the term linear in the Γ_i's as the single-scattering term (the nucleon–nucleon amplitude) for nucleon–nucleus scattering. In general, one finds that the term linear in χ dominates the small $|t|$ scattering. As $|t|$ increases, the χ^2 term begins to dominate and successively the χ^3 term and the higher-order terms become dominant. In other words, here one formally describes two-body large $|t|$ scattering in terms of a succession of small $|t|$ scatterings or multiple scatter-

* For examples, see Chou and Yang (1968a; 1968b); Chiu and Finkelstein (1968a; 1969); Frautschi and Margolis (1968a; 1968b).

ing, provided one formally refers to the term linear in χ as the single-scattering term. Furthermore (we shall discuss this in some detail later), it turns out that if one identifies χ as some appropriate Regge-pole contribution, then terms associated with χ^2, χ^3, $\cdots$ can be interpreted as contributions involving the exchange of two Reggeons, three Reggeons, $\cdots$.

The Glauber theory for nucleon–nucleus scattering is usually referred to as a multiple-scattering model. For our present discussion we shall also refer to those phenomenological models constructed from Eq. (3.18), or analogous series, as multiple-scattering models. As we have stressed for these latter cases, one describes two-body hadron collisions in terms of successive small $|t|$ scatterings or, sometimes, more specifically, in terms of the exchange of single and multiple Reggeons.

4. MULTIPLE-SCATTERING MODELS AND REGGE CUTS

A. Eikonal Approximation and Regge Cuts

In the last section, we saw that the amplitude f can be expressed in the impact-parameter representation, and in eikonal approximation the eikonal function is expressed as an integral over the potential. We do not really know what a potential in high-energy physics is. Arnold suggested a prescription for the potential (1967; 1968; see also Arnold and Blackmon, 1968); he proposed that the Regge-pole contributions be identified with the eikonal function. At this state, the theoretical justification behind such a procedure is not at all clear. Nevertheless, as mentioned in the last section, if one proceeds to make such an identification, then in the expression

$$f=-ip\sum_{n=1}^{\infty}\left\langle\frac{(i\chi)^n}{n!}\right\rangle, \tag{4.1}$$

terms with $n\geq 2$ in the sum have the analytic structure of Regge cuts. In particular, they have the same general cut properties as those deduced from Feynman diagram models and also from the analysis of multiparticle discontinuity formulas. We list some of these properties here.*

(1) The position of the leading branch point corresponding to the exchange of n identical trajectories $\alpha(t)$ (with reasonable shape) is given by

$$\alpha_{\text{cut}}{}^{(n)}(t)=n\alpha(t/n^2)-n+1. \tag{4.2}$$

(2) The contribution of the cut to the amplitude at large s behaves like

$$A_{\text{cut}}{}^{(n)}(s,t)\to\{\Gamma_n(t)s^{[\alpha_{\text{cut}}{}^{(n)}(t)-1]}/(\log s)^{n-1}\}\times[1+O(1/\log s)]. \tag{4.3}$$

(3) Each cut taken to the leading power in s has a definite signature factor. The signature of the cut equals the product of the signature of the Regge poles exchanged.

(4) When each of the n poles is the Pomeranchon, the signs of the discontinuities alternate with n, i.e., Γ_n contains a factor $(-1)^n$.

Cuts generated by the prescription of the eikonal approximation, although satisfying the above properties, are a very special case of all possible solutions. *A priori*, it is not clear why this particular prescription is relevant. The usefulness of this prescription must be tested experimentally. Later on, we shall also mention some other multiple-scattering prescriptions for generating Regge cuts and shall discuss the similarities and the differences between them. As we shall see in Secs. 5 and 6, this general approach for including the multiple-scattering corrections or the cut contributions appears to be favored by the data.

Let us consider Eq. (4.1) in some detail, when the single-scattering term is imaginary. Here we write $\chi(b)=ia(b)$, where a is real. From Eq. (4.1),

$$\frac{f}{p}=i\left[\langle a\rangle-\frac{\langle a^2\rangle}{2!}+\frac{\langle a^3\rangle}{3!}-\cdots\right]. \tag{4.4}$$

The amplitude f is again imaginary, and the multiple-scattering sequence alternates in sign from term to term. This sign alternation plays the crucial role of generating the oscillatory diffraction pattern in the differential cross section. Anselm and Dyatlov (1967) were the first to observe that the Regge-cut sequence associated with multi-Pomeranchon exchange, which has the same sign alternation as deduced from the analysis of multiparticle discontinuity formulas of Gribov *et al.* (1965) (and is also present in the Feynman diagram model), should cause the oscillatory pattern in the differential cross section. They emphasized that the oscillatory pattern is generally expected over a wide range of assumptions about the discontinuities across the Regge cuts. They also pointed out that one expects the $\exp[-(-t)^{1/2}]$ behavior in the large $|t|$ region. To ensure this t dependence, the numerical coefficient C_n, analogous to $1/n!$ in Eq. (4.1), has to be in the range between $1/n!$ and a constant. This specific t dependence had also been obtained previously by Amati *et al.* (1963) and Contogouris (1966).

B. The Modified Impact-Parameter Representation

In the eikonal approximation, the integral over the potential V is contained in the exponent which turns out can easily lead to undesired singularities in the amplitude. Blankenbecler and Goldberger (1962) suggested the following modifications of the impact-parameter representation. They write

$$f=-ip\left\langle\frac{i\chi}{1-(i\chi/2)}\right\rangle=-ip\sum_{n=1}^{\infty}\left\langle\frac{(i\chi)^n}{2^{n-1}}\right\rangle. \tag{4.5}$$

* Mandelstam, 1963; Polkinghorne, 1963; 1965; 1968a; 1968b; Gribov, 1968; Gribov, Pomeranchuk, and Ter-Martirosyan, 1965. For a summary on Regge-cut properties, see also Chiu and Finkelstein, 1968a.

Here χ is the same eikonal function as defined in Eq. (3.13). By comparing Eq. (4.5) with Eq. (4.4), one sees that for the parametrization of multiple-scattering series, the two expressions are identical except for the coefficient $1/n!$, which is now replaced by $1/2^{n-1}$. For $n\leq 2$, the two coefficients are the same; they are different beyond $n=2$. Thus, Eq. (4.5) gives an alternative prescription for including different cut contributions for $n>2$.

Arbarbanel *et al.* (1968a; 1968b) have parametrized the multiple-scattering effect using an expression analogous to Eq. (4.5) with a real single-scattering term (see Sec. 5.A). The effect of multiple scattering here is quite different when compared with an imaginary single-scattering term. Denoting $\chi=a$, one obtains from Eq. (4.5)

$$f(s,t)/p=\langle a\rangle+i\langle a^2\rangle/2-\langle a^3\rangle/4+\cdots, \quad (4.6)$$

which is similar to Eq. (4.4). Here each multiple-scattering term is 90° out of phase with respect to the adjacent terms. As a result, there are no appreciable cancellations and the multiple-scattering effects were found to be weak. Also, no diffraction patterns are observed. In the terminology of optics, a real phase shift is associated with the scattering of light waves through some nonabsorptive medium and no diffraction effects are expected.

C. Iterations of the Unitarity Equation

The scheme of formulating a multiple-scattering model from iterations of the unitarity equation was first considered by Amati, Cini, and Stanghellini (1963). Here,

$$\operatorname{Im} f_l=\operatorname{Im} R_l+pf_lf_l^* \xrightarrow{\text{1st order}} \operatorname{Im} R_l+p|R_l|^2, \quad (4.7)$$

where R_l is the contribution of a Regge pole. It was emphasized by Finkelstein and Jacob (1968) that the iterative series thus obtained for the case $\chi=ia$ as considered in Eq. (4.4) does not have the sign alteration. This is contrary to the results deduced, for example as mentioned in Sec. 4.A, from Feynman diagram models for the Regge cuts. As discussed in Appendix B, this is also not favored by experiment. We will not pursue this prescription any further.

D. The Quark Model

Nucleon–nucleon scattering and other two-body hadron collisions have also been discussed in terms of the multiple scattering of quarks. Here the quark–quark amplitude is the actual single-scattering amplitude. This single amplitude is to be interpreted in the literal sense as the nucleon–nucleon amplitude in the Glauber theory for the nucleon–nucleus scattering. We shall not discuss this model here, but simply refer the reader to a recent paper by Harrington and Pagnamenta (1968). In this paper, the authors have fomulated a multiple-scattering model within the framework of the quark model and have applied their model to various elastic-scattering processes over a wide angular range.

Let us sum up our discussion here: In this section we are mainly concerned with the problem of formally generating a multiple-scattering series from some formally identified single-scattering amplitude. This can be achieved, for example, by using the eikonal approximation, the modified impact-parameter representation, or iterations of the unitarity equation. As mentioned, the first two procedures are similar, while at this stage the last one is not preferred. Instead of using a specific prescription for generating the multiple scattering series, as mentioned in Sec. 4.A, Anselm and Dyatlov followed a different approach. They parametrized this series, using the knowledge of the properties of Regge cuts as deduced from Feynman diagram models. A significant range of flexibility is allowed in their parametrization. In spite of this flexibility, they were able to deduce the general qualitative features of the multiple-scattering amplitude, such as the oscillatory behavior and the $\exp[-(-t)^{1/2}]$ dependence in the large $|t|$ region. However, for more quantitative description of the data, this latter approach seems to provide too much freedom. We note that the multiple-scattering model, following specific prescriptions such as the eikonal approximation, has been considered by various authors and seems to be promising. In Secs. 5 and 6 we shall discuss phenomenology using the multiple-scattering model, mainly within the framework of the eikonal approximation.

5. APPLICATIONS OF THE MULTIPLE-SCATTERING MODEL TO ELASTIC AND LARGE $|t|$ INELASTIC SCATTERING

In this section we are concerned with the application of the multiple-scattering model, especially in the nonforward region where the asymptotic theory of Chou–Yang is particularly inadequate (see Sec. 3.B and Fig. 13). We shall discuss the application of elastic scattering in Secs. 5.A–5.D and to the inelastic scattering in Sec. 5.E.

A. The Single-Scattering Amplitude

Parametrizations of the single-scattering amplitude for elastic scattering can be grouped into four categories. We consider these four cases in some detail here.

(1) *The Optical Amplitude*

Since multiple elastic scatterings occur at a fixed energy, one can discuss the multiple-scattering amplitude at any given energy. A convenient and crude parametrization for the single-scattering amplitude is of the form

$$f_B/s^{1/2}=ic\exp(at), \quad (5.1)$$

where for simplicity one assumes a and c to be real, although in general they need not be. Contogouris (1966) has used Eq. (5.1) to analyze large $|t|$ pp, πp,

and $\bar{p}p$ data. He found that the qualitative behavior of the differential cross section in the large $|t|$ region can be plausibly correlated with the small-angle scattering parameters. At different energies these parameters are, in general, different. To proceed from here, one would incorporate the energy dependence explicitly into Eq. (5.1).

(2) *The Pomeranchon Exchange Amplitude*

Here one incorporates the energy dependence into Eq. (5.1) by Regge theory. The single-scattering amplitude here has the form

$$f_B/s^{1/2}=cs^{\alpha-1}\exp[i\pi(1-\alpha/2)], \tag{5.2}$$

with

$$\alpha=1+\alpha' t. \tag{5.3}$$

This form was considered by Amati *et al.* (1963) in the context of iterations of unitarity equations and later by Anselm and Dyatlov (1967) in connection with the Regge-cut series. Recently this form has been discussed extensively by Frautschi and Margolis (1968a; within the framework of the eikonal approximation. The parametrization of Frautschi and Margolis is summarized in Appendix B. As discussed there and also in Sec. 5.B, although the multi-Pomeranchon exchange amplitude so obtained has energy dependence, it still only gives a crude approximation to the scattering amplitude near $t=0$, since it gives the wrong sign for the ratio of real part to imaginary part of the forward scattering amplitude and the wrong energy dependence for the total cross section. Also, since $\alpha'\neq 0$, the significance of the Chou–Yang asymptotic theory is not clear in this model.

(3) *The Hybrid Model*

This model was suggested by Finkelstein and the author (Chiu and Finkelstein, 1968a) and also independently by Arnold and Blackmon (1968). The latter authors were concerned mainly with the small $|t|$ phenomenology, while the former authors were concerned with the larger $|t|$ region as well. To retain the Chou–Yang asymptotic theory, to remedy the discrepancies mentioned in (2), and to minimize the parameters associated with the Pomeranchon contribution, we write

$$f_B/s^{1/2}=P+R, \tag{5.4}$$

where P denotes the contribution of the Chou–Yang type (which we formally call the "Pomeranchon" contribution) and R the proper Regge-pole contribution. In terms of the multiple-scattering picture, schematically,

$$f/s^{1/2}=P^n+(R+RP^n)+(RR+RRP^n)+\cdots, \tag{5.5}$$

where P^n denotes the sum of all the terms involving pure Pomeranchon exchanges and is the asymptotic amplitude. The RP^n term denotes the sum of all the multiple-scattering terms which are linear in R. The RRP^n term denotes those bilinear in R, etc. In practice, the parameters of P are given by the Chou–Yang model and those of R are left to be determined through fits to the data. We shall defer further discussion on the applications of the hybrid model until Secs. 5.C and 5.D.

(4) *The Multi-Regge-Pole Amplitude*

In principle the P term in Eq. (5.4) does not have to be a fixed pole, i.e., with $\alpha'=0$, where $\alpha(t)=1+\alpha' t$. Frautschi and Margolis (1968a) suggested instead, $\alpha_P'\approx 1$ GeV^{-2}. Here one is obliged to determine the parameters of P and those of the secondary trajectories simultaneously. A more elaborate analysis work comparable to (3) above is required. No results are available at this stage.

The amplitude of Arbarbanel *et al.* (1968b) again has two pole terms. However, it differs somewhat from both (3) and (4) mentioned above. We shall comment on it here. They assume that the pp amplitude is dominated by a local current–current term h_c plus a diffraction term h_D. To unitarize the amplitude, they write

$$\frac{iT}{(4\pi)^{1/2}}=\left\langle\frac{h_c+h_D}{1-(h_c+h_D)}\right\rangle$$

$$=\left\langle\frac{h_D}{1-h_D}+\frac{h_c}{(1-h_D)(1-h_c-h_D)}\right\rangle, \tag{5.6}$$

with

$$h_D/(1-h_D)=\langle-(\alpha+\beta i)\exp(t/R^2)\rangle, \tag{5.7}$$

$$h_c=\langle(iAG_{M_p}{}^2/(4\pi)^{1/2}\rangle; \tag{5.8}$$

α, β, R, and A are the parameters and G_{M_p} the proton magnetic form factor. In the context of multiple scattering, Eq. (5.6) implies that they have treated the term $\langle h_D/(1-h_D)\rangle$, rather than $\langle h_D\rangle$, as the single-scattering term. In the limit $h_c\gg h_D$, the multiple-scattering series is given by

$$iT/(4\pi)^{1/2}\approx\langle\sum_{n=1}^{\infty}h_c{}^n\rangle, \tag{5.9}$$

which is comparable to Eqs. (4.4) and (4.6).

The calculated differential cross section of Arbarbanel *et al.* (1968b) is indicated as the solid curve in Fig. 15. For large $|t|$ this curve differs insignificantly from the term $0.4G_M{}^4$. Also, no oscillatory pattern is present in the calculated differential cross section. These authors emphasized that the calculated differential cross section is essentially explained by the single-scattering term; the multiple-scattering effects are not important. Presumably, these features are closely tied to the fact that the term h_c/i is real, as discussed in Sec. 4.B. They pointed out that the curves in Fig. 15 fit the observed pp differential-cross-section data at $s\approx 60$

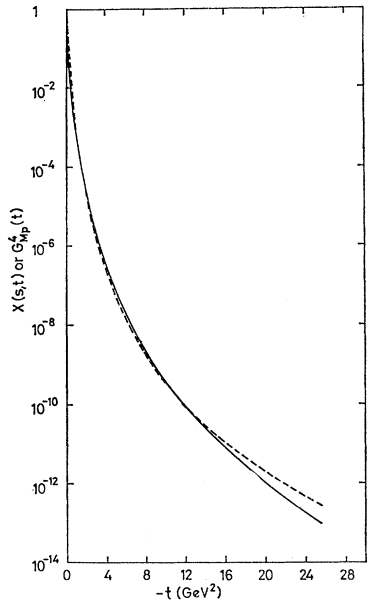

FIG. 15. The comparison between the calculated differential cross section given by Arbarbanel *et al.* and the contribution of the proton form factor, G_{Mp}^4. The solid curve is the calculated differential cross section and the dotted curve is the form factor G_{Mp}^4 (from Arbarbanel *et al.*, 1968b).

GeV² to within a factor of ≈2–3 over the measured range out to $|t| \approx 15$ GeV².

In principle, the same model can also be applied to $\bar{p}p$ scattering with the sign of h_c reversed. Since this h_c term contributes significantly near $t=0$, with the sign change noticeable effects will be expected in $\bar{p}p$ scattering in the same t region. So far in high-energy phenomenology, there has been no convincing evidence for introducing an *odd* signature amplitude with $\alpha(0)=1$. It would be interesting to look for experimental evidence to investigate this possibility. The presence of such an odd signature amplitude would imply, for example, at asymptotic energies

$$(\text{Re/Im})\,(pp) = -\,(\text{Re/Im})\,(\bar{p}p) \neq 0.$$

B. The Multi-Pomeranchon Exchange Model

In this section we take a close look at the work of Frautschi and Margolis (1968a). They have applied the multi-Pomeranchon exchange model using the eikonal approximation to pp, $\bar{p}p$, and πp data. Their parametrization, as mentioned earlier, is summarized in Appendix B. In Fig. 16 we show their best fit to the pp differential cross section. Their calculated differential cross section has about the right exponential falloff at large $|t|$; it shrinks suitably and has the "break" near $t=-1.2$ GeV². The fit looks encouraging. One expects that the quality of the fit will be improved with the inclusion of the proper trajectory contributions.

As emphasized by various authors (Chiu and Finkelstein, 1968a; Frautschi and Margolis, 1968a) and also discussed in Appendix B, the multi-Pomeranchon amplitude obtained from the eikonal approximation can, at best, be a crude approximation to the near forward scattering. For example, it has the following discrepancies as compared with the data:

(1) The ratio of real part to imaginary part of the forward amplitude is calculated to be positive, whereas the data for pp scattering is $\sim -20\%$.

(2) The calculated pp total cross section increases slightly with the increase of energy while the data decreases slightly.

We mention here that the quantity $(\sigma_{\bar{p}p}-\sigma_{pp})/\sigma_{pp} \approx 0.2$ at 20 GeV/c, whereas in a multi-Pomeranchon exchange model this difference should be zero. In the next section, we shall discuss phenomenology with the inclusion of the secondary trajectory's contribution. As we shall see, with this modification the above discrepancies are overcome. Furthermore, within the framework of the hybrid model, the features of the Chou–Yang asymptotic theory are retained.

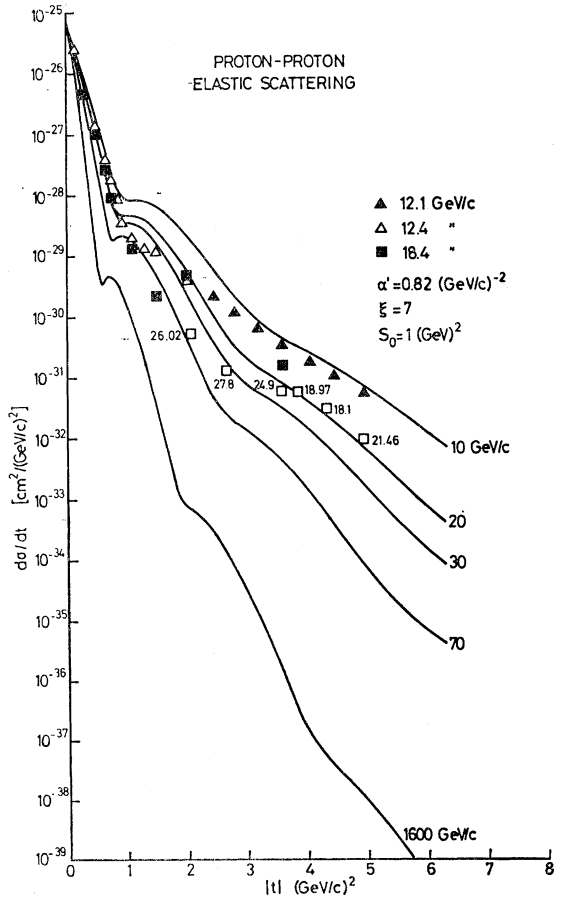

FIG. 16. The pp differential cross section calculated by Frautschi and Margolis using the multi-Pomeranchon exchange model. The data points are included for comparison (from Frautschi and Margolis, 1968a).

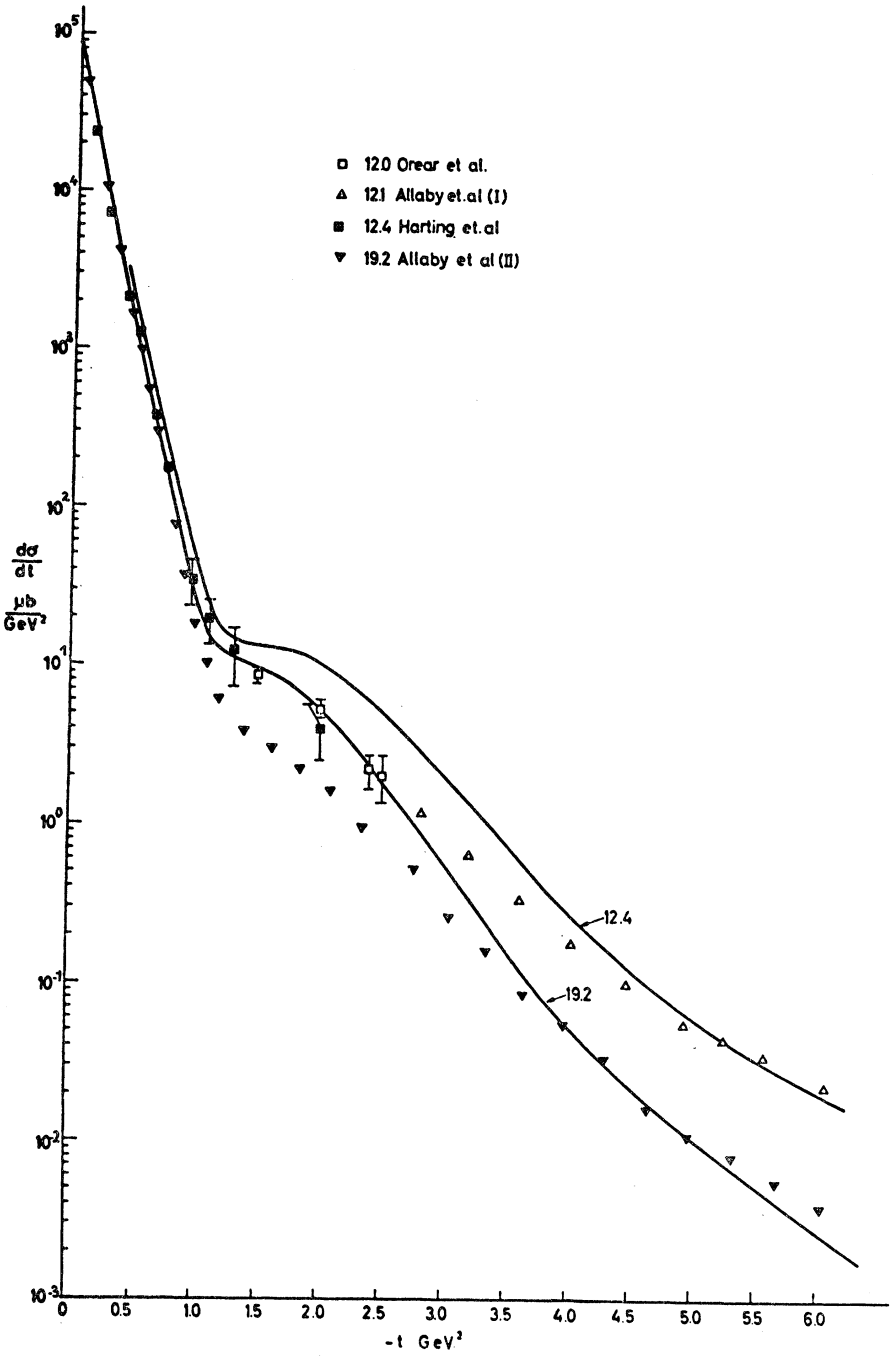

FIG. 17. The fit to pp differential cross section using the hybrid model (from Chiu and Finkelstein, 1969).

C. Application of the Hybrid Model to pp and $\bar{p}p$ Scattering

This work is by Finkelstein and the author (1968a; 1969). Here we take P of Eq. (5.4) to be essentially that given by Durand and Lipes (1968), and R to be dominated by the f^0 and ω^0 trajectories, with $\alpha=\frac{1}{2}+t$. We assume that f^0 and ω^0 are exchange degenerate, so that R is real. One can see this readily, since

$$R(s,t)=f^0-\omega^0=\{[-1-\exp(i\pi\alpha)]-[1-\exp(i\pi\alpha)]\}bs^{\alpha-1}=-2bs^{\alpha-1}. \quad (5.10)$$

Our fit is illustrated in Fig. 17. The curves reproduce the general trend of the t dependence and indicate the presence of structure near $t=-1$ GeV². The calculated

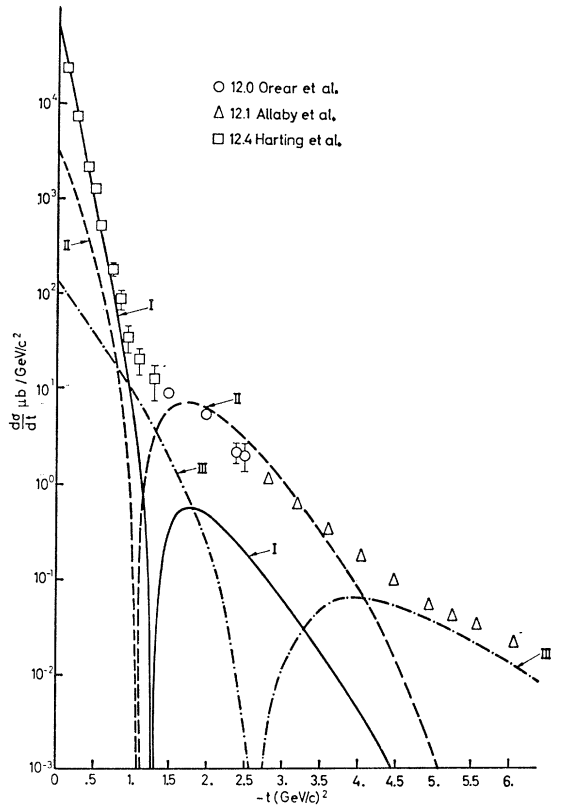

FIG. 18. Decomposition of the contribution to the pp differential cross section from various multiple-scattering terms in the hybrid model: curve I$=P^n$, II$=(R+RP^n)$, and III$=(RR+RRP^n)$ (from Chiu and Finkelstein, 1968a).

energy dependence of the differential cross section is reasonable. The detailed decomposition of the contribution due to various terms in Eq. (5.5) is shown in Fig. 18. Curve I corresponds to the asymptotic contribution; II, to terms linear in R; and III, to terms bilinear in R. One sees that *the breaks in the slope of the pp differential cross section are directly correlated with the dominance of these three contributions.*

In order to calculate the $\bar{p}p$ differential cross section, we reverse the sign of the ω^0. More explicitly, in analogy to Eq. (5.10),

$$R(s,t)=f^0+\omega^0=\{(-1-\exp(-i\pi\alpha)] +[1-\exp(-i\pi\alpha)]\}bs^{\alpha-1}=-2b\exp(-i\pi\alpha)s^{\alpha-1}. \quad (5.11)$$

We do not expect that the $\bar{p}p$ differential cross section predicted from our solution would fit the data. However, there are several qualitative features worth pointing out.

(1) At $t=0$, the $\bar{p}p$ differential cross section is larger than the pp differential cross section, and the total cross section for $\bar{p}p$ is also larger than that for pp. These properties can easily be seen from Eqs. (5.10), (5.11), and (5.4).

(2) The $\bar{p}p$ forward peak is sharper than the pp peak. The crossover point for pp and $\bar{p}p$ differential cross sections is at $t=-0.37$ GeV², as compared to $t=-0.2$ GeV² in the data (Foley *et al.*, 1965). In a pure Regge-pole model, one cannot get this crossover point without violating factorization (Chan, 1968).

(3) The diffraction pattern in the $\bar{p}p$ differential cross section is more pronounced than that for the pp differential cross section. In fact, a dip is observed in the calculated differential cross section at $t\approx-0.65$ GeV² and $P_L=12$ GeV/c. As energy increases, the dip moves to the larger $|t|$ region, and it is at $t=-1.3$ GeV² at the asymptotic energy. The experimental dip positions in the $\bar{p}p$ differential cross section are as follows (see Figs. 9 and 19):

P_L (GeV/c)	t (GeV²)
5.9	~-0.5,*
8	~-0.6,†
16	~-0.8.†

The shift of the dip is quite pronounced here.

There is an amusing relation which is obeyed by the pole terms, approximately obeyed by the multiple-

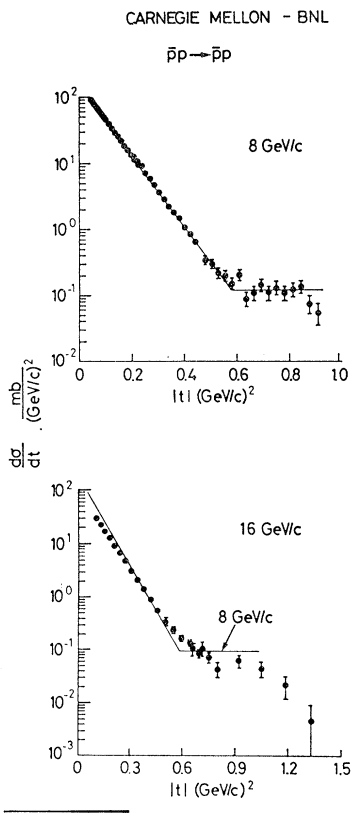

FIG. 19. Differential cross section for $\bar{p}p$ elastic scattering at 8 and 16 GeV/c. The full curves on both plots show the behavior of the 8-GeV/c data (from Bellettini, 1968; and Birnbaum *et al.*, 1968).

* The $\bar{p}p$ data. Cornell–BNL collaboration (see Ashmore *et al.*, 1968; Orear *et al.*, 1968a); Böckmann *et al.*, 1966; Foley *et al.*, 1963b.

† Birnbaum *et al.* (1968).

scattering terms in our model, and which is independent of many of the details of our parametrization. From Eqs. (5.10) and (5.11), one predicts that

$$\mathrm{Re}\, A_{pp}(s, 0)/\mathrm{Im}\, A_{pp}(s, 0) = (\sigma_{pp}{}^{T} - \sigma_{\bar{p}p}{}^{T})/\sigma_{pp}{}^{T}. \quad (5.12)$$

We have used this relation together with the experimental values for $\sigma_{pp}{}^{T}$ and $\mathrm{Re}\, A_{pp}/\mathrm{Im}\, A_{pp}$ to predict $\sigma_{\bar{p}p}{}^{T}$ and compare it with the experimental data. We find that the agreement is satisfactory.

D. Combined Features of the Optical Model and the Regge-Pole Model

From the examples of pp and $\bar{p}p$, one sees that the general features of the elastic scattering predicted by the hybrid model are closely correlated with the phase of the proper Regge amplitude R near the forward direction. In Table I we list the comparison between the situation when R is purely real, such as in the pp case [see Eq. (5.10)], and when it is purely imaginary, such as in the $\bar{p}p$ case [see Eq. (5.11)]. We note that the hybrid prescription includes both the optical model features, (e.g., the blacker the disk, and hence the larger the total cross section, the sharper the peak and the more pronounced the diffraction pattern) and the Regge-pole model features (e.g., the energy dependence of the total cross section and the shrinkage effect). From the KN total-cross-section data one finds that the proper Regge-pole contributions to the K^+p forward amplitude are mainly real, while that to the K^-p forward amplitude are mainly imaginary. [See for example, Phillips and Rarita (1965b).] This in turn implies that the qualitative contrast between the K^+p and the K^-p amplitudes should bear some resemblance to that between the pp and $\bar{p}p$ amplitudes. We recall the experimental data as discussed in Sec. 2.C. One finds this qualitative resemblance is indeed present. Here the K^-p peak shrinks while the K^+p peak expands, and the K^-p peak is sharper than the K^+p peak. Also, oscillatory structure in the K^-p differential cross section has been observed at 5.5 GeV/c, although at 10 GeV/c this structure seems to be much less pronounced (see Fig. 10). At this stage, comparable data for K^+p scattering are not available. This model predicts a relatively smooth differential cross section. It would be interesting to see if future K^+p measurements can verify this prediction. For the $\pi^{\pm}p$ scattering, from the data of the real part of imaginary part of the forward amplitude (Foley *et al.*, 1967), one can easily check that, for both the π^+p and π^-p amplitudes, the proper trajectory contributions lie in the second quadrant of the Argand diagram. One does not expect much contrast between these two differential cross sections, and this agrees with the data. Also, from Table I we find that it is not surprising that the $\pi^{\pm}p$ experimental differential cross section does not show much shrinkage (Foley *et al.*, 1963a).

TABLE I Comparison between the situation when R is purely real, as in the pp case [see Eq. (5.10)], and when R is purely imaginary, as in the $\bar{p}p$ case [see Eq. (5.11)].

Example	pp	$\bar{p}p$
Proper trajectories	$f^0-\omega^0$	$f^0+\omega^0$
Amplitude R near $t=0$	Real	Imaginary
σ_T	$\sim$ Constant	Energy dependent
Shrinkage	Shrinks	Expands
Forward peak	Less sharp	Sharp
Diffraction pattern	Less pronounced	Pronounced

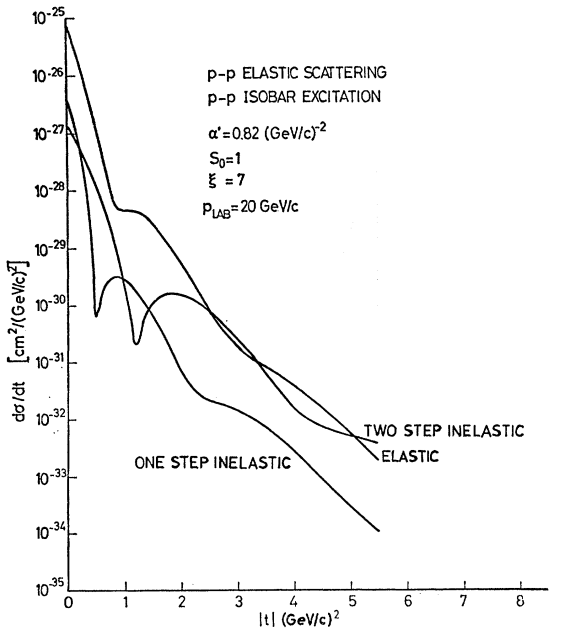

FIG. 20. A comparison between the calculated pp differential cross section and the calculated isobar-production cross section given by Frautschi and Margolis 1968b). The curves for the isobar production differential cross section are calculated with two different assumptions.

E. Multiple-Scattering Features for Large $|t|$ Inelastic Scattering

For large $|t|$ inelastic scattering, one could conjecture that the process proceeds as follows: As two hadrons collide they undergo multiple elastic scattering in the initial state, then a small $|t|$ inelastic transition, and eventually multiple elastic scattering in the final state. If the initial and the final elastic-scattering amplitudes are comparable, then the t dependence in the large $|t|$ region for inelastic scattering will be similar to that for elastic scattering. Frautschi and Margolis (1968b) have studied in some detail the multiple-scattering model for isobar production. Figure 20 indicates the calculated curves for isobar production, involving what they referred to as one-step

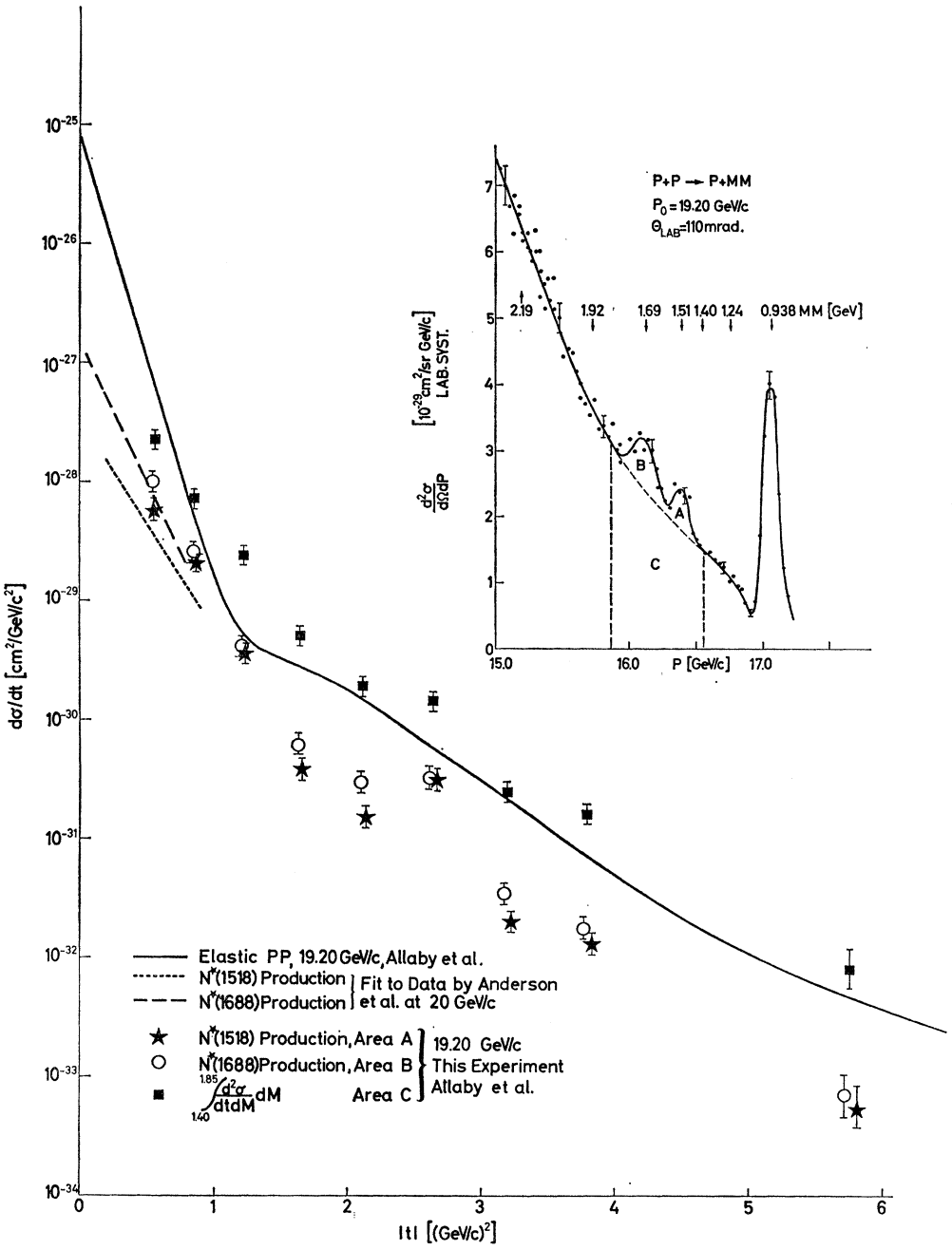

FIG. 21. The comparison between the behavior of pp differential cross section and the isobar-production cross section. The solid curve indicates the experimental pp differential cross section; the points are the experimental isobar-production cross section (from Allaby *et al.*, 1968c).

and two-step inelastic transitions (i.e., $i \to j$ and $i \to m \to j$, respectively, with i, m, j different channels). The elastic differential cross section is illustrated in the same figure for comparison. Beyond $|t| = 1$ GeV^2 the elastic differential cross section and their one-step curve are similar. Beyond $|t| = 2$ GeV^2, the elastic and the two-step curves are similar. The recent CERN data (Allaby *et al.*, 1968c) on N^* (1512) and N^* (1688) production are illustrated in Fig. 21. Note the similarity in the t dependence between the isobar-production differential cross section and the elastic differential cross section. These data support the above interpretation.

6. THE IMPACT OF THE MULTIPLE-SCATTERING MODEL ON HIGH-ENERGY PHENOMENOLOGY

We have seen that the multiple-scattering picture provides a qualitative description of elastic and inelastic scattering in the intermediate $|t|$ region. It also contains the virtues of both the optical model and the Regge-pole model, which account for the general behavior of elastic scattering near the forward direction. Let us proceed to discuss those cases where a pure Regge-pole model describes the data to a first approximation. The multiple-scattering correction to a Regge-pole contribution, to first order in the Regge-pole coupling, is equivalent to the absorptive correction to the same Regge-pole, as discussed by Kimel and Miyazawa (1967), Cohen-Tannoudji, Morel, and Navelet (1967), Squires (1968), and others. This equivalence was emphasised recently by Finkelstein and Jacob (1968). In other words, the effect of the multiple-scattering corrections that we shall be concerned with is equivalent to that of the absorptive corrections and, as we have discussed earlier, to that of the Regge cuts. Since the Regge power law and the nonsense-wrong-signature dips are the two main successes in the phenomenology of the Regge-pole model, we shall investigate the influence of multiple-scattering corrections on both of these aspects.

A. Multiple-Scattering Corrections and the Regge Power Law

Near $t=0$, the power behavior associated with the multiple-scattering correction or the cut [e.g., the RP^n term in Eq. (5.5)] is close to the power behavior of the pole term [e.g., the R term in Eq. (5.5)], and we expect that the energy dependence will not be disturbed. On the other hand, in the large $|t|$ region, the effect of corrections could be important. Rivers (1968) has investigated the influence on the power behavior of a model amplitude caused by the cut corrections. One of his plots of α^{eff} versus t, where α^{eff} is the effective power is shown in Fig. 22. The solid line (a) indicates the input trajectory α_p, the line (b) indicates the branch point associated with the ρP cut, and the dotted lines are the effective power α^{eff} at various energies. For this particular example, the cut contribution does not affect the energy dependence near $t=0$. On the other hand, it completely dominates the energy dependence beyond $t=-0.4$ GeV^2. We do not suggest that the quantitative features are necessarily relevant to the physical situation. Nevertheless, this calculation at least hints that, in the large $|t|$ region, because of the presence of multiple-scattering corrections, the situation could be complicated.

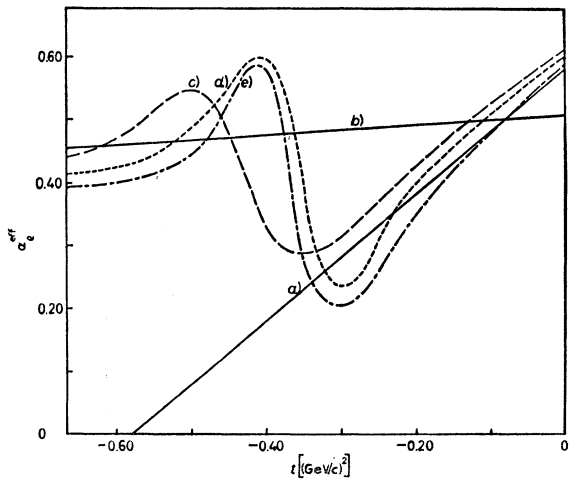

FIG. 22. The effective power law for a model amplitude at various energies calculated by Rivers. Curve a is the input ρ trajectory; curve b is the branch point associated with the $\rho\rho$ cut. The dotted curves are the effective power law obtained at different energies (from Rivers, 1968).

Let us now discuss the physical trajectory functions in some detail. From Regge-pole models* one has

$$\alpha_\rho = 0.57 + 1.0t,$$
$$\alpha_{A_2} = 0.34 + 0.35t. \tag{6.1}$$

The A_2 trajectory function quoted here was determined by Phillips and Rarita from the $\pi^- p \to \eta^0 n$ differential-cross-section data.† Due to the inaccuracy of the data, this trajectory function is poorly known at present. For example, Arbab, Bali, and Dash (1967) showed that the energy dependence of the data is also compatible with the trajectory function

$$\alpha_{A_2} \approx 0.5 + 0.85t. \tag{6.1a}$$

With the inclusion of the multiple-scattering correction, Henyey *et al.* (1968) obtained

$$\alpha_\rho = 0.37 + 1.2t, \tag{6.2}$$

whereas Arnold and Blackmon (1968) gave

$$\alpha_\rho = 0.50 + 0.80t,$$
$$\alpha_{f^0} = 0.47 + 1.0t. \tag{6.3}$$

With the assumption of the extended-exchange-degeneracy hypothesis (Harari, 1968; also Freund, 1968) one predicts that

$$\alpha_\rho = \alpha_{f^0} = \alpha_{\omega^0} = \alpha_{A_2} \approx 0.44 + 0.93t, \tag{6.4}$$

where the trajectory function is obtained by a linear extrapolation from the physical mass spectra. (Chiu and Finkelstein, 1968b). Taking into account the experimental uncertainties of the data and also the extra degree of freedom due to the inclusion of the cut con-

* Höhler, Schaile, and Sonderegger (1966), Arbab and Chiu (1966), Phillips and Rarita (1965a), and Arbab, Bali, and Dash (1967).

† Phillips and Rarita (1965a).

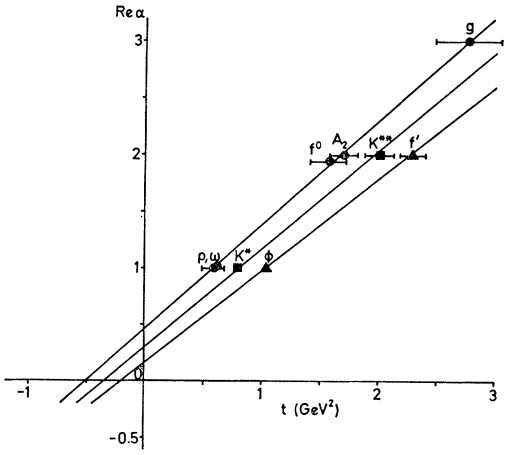

FIG. 23. The degenerate trajectories suggested by Chiu and Finkelstein (1968b).

tribution, we are led to conjecture the approximate validity of Eq. (6.4) in the $t<0$ region, and perhaps a similar possibility for the other vector and tensor trajectories. According to the extended-exchange-degeneracy hypothesis (Harari, 1968) the vector and tensor nonets are divided into three groups:

$$(\rho, \omega, A_2, f^0), \quad (K^*, K^{**}), \text{ and } (f^{0\prime}, \phi).$$

In the linear approximation, these three groups are respectively described by

$$\alpha^{(\mathrm{I})}(t)\approx 0.44+0.93t,$$

$$\alpha^{(\mathrm{II})}(t)\approx 0.29+0.87t,$$

and

$$\alpha^{(\mathrm{III})}(t)\approx 0.15+0.82t.$$

This situation is illustrated in Fig. 23 (Chiu and Finkelstein, 1968b). It will be interesting to see if the present high-energy data are consistent with this relatively simple picture of the Regge trajectories.

B. Multiple-Scattering Corrections and the Dip-Bump Structure in the Differential Cross Section

(1) *The π^+p Backward Differential Cross Section*

We recall the pronounced dip in the π^+p differential cross section near $u=-0.16$ GeV, which was explained in the Regge-pole model (Chiu and Stack, 1967) as due to the nucleon trajectory passing through a nonsense-wrong-signature point, $\alpha_N=-\frac{1}{2}$. Since then, the experimental data have been greatly improved in accuracy and have become available at higher energies. These results further confirm this interpretation (Orear, 1968b; Barger and Cline, 1968). Following Chiu and Finkelstein (1969), we would like to show that the multiple-scattering correction does not obscure this simple interpretation. This is due to the fact that the zero in the nucleon amplitude at $\alpha_N=-\frac{1}{2}$ is close to the backward direction; this in turn causes the multiple-scattering correction to be relatively small near the dip region. In Fig. 24, we illustrate the results, where the solid curve stands for the pole term alone. The dotted line is the differential cross section after the inclusion of the multiple-scattering correction. We note that the position of the dip is essentially not shifted, as expected, and that the secondary peak is greatly suppressed. Leaving the trajectory function as before, we readjusted the u-dependent parameter in the residue function. The result is illustrated in Fig. 25. We see that, even with the inclusion of the multiple-scattering correction, fits to the data for $u\gtrsim -0.8$ GeV^2 are still adequate.

(2) *The $\pi^-p\to\pi^0n$ Differential Cross Section*

Recently, Henyey *et al.* (1968) suggested that the dip in the $\pi^-p\to\pi^0n$ differential cross section near $\alpha_\rho=0$ can be generated by an absorption mechanism alone or, in our language, by the multiple-scattering correction alone. To demonstrate this effect, they chose to parametrize the spin-flip amplitude of the ρ, B_ρ, such that it does not vanish at $\alpha_\rho=0$. Their fit to the data is illustrated in Fig. 26. The data are not fitted in the χ^2 sense. In fact the contribution of the nonflip amplitude of the ρ is not included in the calculated differential cross section. Also, they had to multiply the ab-

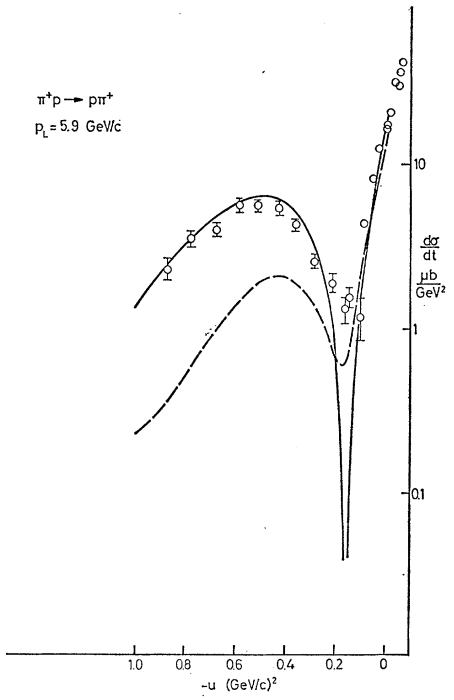

FIG. 24. The π^+p backward differential cross section versus u. The solid curve corresponds to a fit with the nucleon contribution alone, with $\alpha_N=-0.34+u$. The dashed curve indicates the differential cross section after the inclusion of the multiple-scattering correction, with the same trajectory function (Chiu and Finkelstein, 1969).

sorption correction by a factor of 2 to fit the data. In spite of these adjustments, their dip–bump structures look impressive. Needless to say, the same angular distribution has been fitted in the past by the ρ trajectory alone* and by the ρ trajectory plus the multiple-scattering correction† having $B_\rho \neq 0$ at $\alpha_\rho = 0$. The latter fit, shown in Fig. 27, is given by Arnold and Blackmon (1968) using the hybrid prescription. It seems likely, as far as the dip and secondary bump structure for the $\pi^- p \to \pi^0 n$ differential cross section is concerned, that both the nonsense-wrong-signature mechanism and the diffraction mechanism are operating.

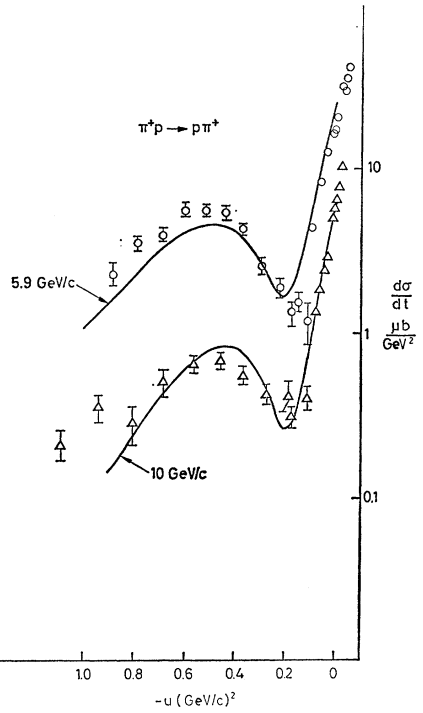

FIG. 25. A fit to the $\pi^+ p$ differential cross section with the inclusion of the multiple-scattering effect, where we keep the same trajectory function, $\alpha_N = -0.34 + u$, as was used for the Regge-pole fit (from Chiu and Finkelstein, 1969).

(3) *Dips in $\bar{p}p$ Differential Cross Section*

In the hybrid model, the presence of this dip is related to the diffraction effect. As mentioned before, since $\sigma_{\bar{p}p} > \sigma_{pp}$, the diffraction phenomenon in $\bar{p}p$ scattering is expected to be more pronounced than that in pp scattering. In the language of the optical model, this means that the blacker the disk, the sharper the peak and the more pronounced the diffraction pattern. As the energy increases, the disk becomes less black and as a result the diffraction peak is broader. It is interesting to recall that in the Regge-pole model, this dip–bump structure is mainly due to a delicate interference between P and ω^0 in the region where the contribution of the P' (or f^0) is relatively unimportant. As the energy increases, one also expects the dip to move slowly to the larger $|t|$ region (Chiu, Chu, and Wang, 1967; Barger, 1968).

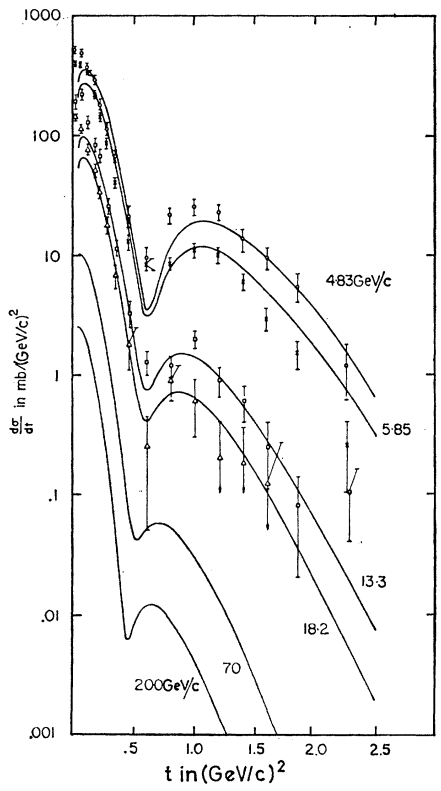

FIG. 26. The fit to $\pi^- p \to \pi^0 n$ differential cross section by Henyey *et al.* (1968).

To sum up, with the introduction of the multiple-scattering picture, in addition to the nonsense-wrong-signature zeros and the interference effects between different Regge-pole amplitudes, diffraction effects can also lead to the dip–bump structure. Consequently, one has to be more cautious about explaining the

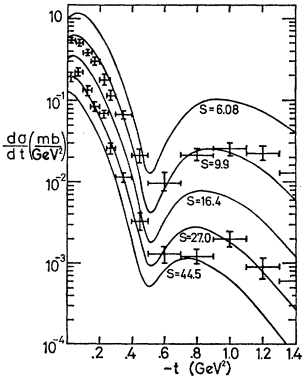

FIG. 27. The fit to $\pi^- p \to \pi^0 n$ differential cross section by Arnold and Blackmon (1968).

* Höhler, Schaile, and Sonderegger (1966); Arbab and Chiu (1966).

† Arnold and Blackmon (1968); Kimel and Miyazawa (1967); Cohen-Trnnoudji, Morel, and Navelet (1967).

structure of the differential cross section. As $|t|$ increases, the multiple-scattering correction becomes more and more important. We observe that it seems unlikely that the dip structure in the differential cross section beyond $t=-1$ GeV^2 can be directly associated with specific values of α. On the other hand, we have given a concrete example, that of π^+p backward scattering, where the dip near $u=-0.16$ GeV^2 is still interpreted as due to $\alpha_N=-\frac{1}{2}$.

C. The Role of the Multiple-Scattering Model and High-Energy Phenomenology

The role of introducing the multiple-scattering idea in high-energy phenomenology can hardly be overestimated.

(1) It provides a model for large $|t|$ scattering. We have discussed the work of Chou and Yang and of Durand and Lipes, where they explain the asymptotic pp differential cross section in terms of an optical-diffraction model, which is equivalent to the multiple-scattering model. We have illustrated that the multiple-scattering picture gives a qualitative description of scattering in the intermediate-momentum-transfer region, such as for pp elastic scattering and isobar-production scattering.

(2) It contains features from both the optical model and the Regge-pole model: In this model the magnitude of the total cross section is correlated with features of the diffraction pattern and the energy dependence is correlated with the parameters of the proper Regge poles. Within the prescription of the hybrid model, the shrinkage, antishrinkage and nonshrinkage effects arise automatically. We have seen that these features are in a qualitative agreement with present pp, $\bar{p}p$, $\pi^{\pm}p$, and $K^{\pm}p$ elastic data. This model predicts a relatively smooth K^+p differential cross section in the large $|t|$ region. It would be interesting to see if the future K^+p measurement can verify this prediction.

(3) To the first order in the proper Regge-pole couplings, the multiple-scattering model is the absorption model. As an absorption model, it helps to explain problems encountered in the Regge-pole model, such as the crossover effect, the nonzero polarization in $\pi^-p\to\pi^0n$ scattering, and it provides the peak in the $pn\to np$ differential cross section without introducing conspiracy, etc.

(4) It essentially preserves the Regge power law near $t=0$ (or $u=0$), which has been proved to be relatively successful experimentally (Chan, 1968).

(5) It provides a more general explanation of the dip–bump structure in the differential cross section. Within the Regge-pole model this structure comes from either the nonsense-wrong-signature zero in a Regge amplitude or from the interference effect between different Regge amplitudes. However, multiple-scattering corrections can also generate a dip–bump structure. Thus one has to be particularly cautious and consider these various possibilities in explaining this structure in the differential cross section. We have seen that for the dip in the π^+p backward differential cross section, the explanation within the framework of the multiple-scattering model remains the same as that in a pure Regge-pole model.

(6) It reopens possibilities for simple Regge trajectory functions. We have mentioned the possibility of the approximate exchange degeneracy among various trajectories. We recall that, in fitting the secondary bump structure in $\pi^{\pm}p$ elastic scattering (Chiu, Chu, and Wang, 1967) within the framework of the Regge-pole parameterization, it was necessary to introduce a curved trajectory for the P'. Similarly, curved trajectories were also introduced for N and Δ (Barger and Cline, 1968) in order to analyze the backward $\pi^{\pm}p$ differential cross section in the large $|u|$ region. With the introduction of multiple-scattering effects in the large $|t|$ (or $|u|$) region, the multiple-scattering term is generally more important that the single-scattering term. Thus the requirement of a curved trajectory is no longer necessary. We speculate that the data could tolerate linearly falling trajectories in the negative t region, in analogy to the linearly rising trajectories observed in the positive t region.

Recently, Frautschi and Margolis suggested that with the introduction of multiple-scattering corrections there might be a possibility that $\alpha_p'\approx 1$ GeV^{-2}. This is not obvious since, in the small $|t|$ region (e.g. $|t|\approx 0.5$ GeV^2) at our present energies, the shrinkage rate associated with Pomeranchon exchange when the multiple-scattering effect is included is about the same as that for single Pomeranchon–pole exchange alone. Nevertheless, they argued that the role of the secondary trajectories is expected to be somewhat different from that in a Regge-pole model. It would be interesting to find out if quantitative fits to the experimental data can be achieved in the future with $\alpha_p'\approx 1$ GeV^{-2}.

APPENDIX A: THE FIXED-ANGLE LOWER BOUND AND THE ASYMPTOTIC ANGULAR DEPENDENCE

1. The Generalized Cerulus–Martin Fixed-Angle Lower Bound

The Cerulus–Martin fixed-angle lower bound for pp scattering is given by

$$f_{\mathrm{LB}}(s,\cos\theta_s)\xrightarrow[s\to\infty]{\text{fixed }\theta_s}\exp\left[-C(\theta_s)s^{1/2}\ln s\right]. \quad \text{(A1)}$$

To arrive at Eq. (A1), they assumed: (1) the amplitude f is analytic within some domain D in the z plane,

with the boundary of D tangential to the real axis at the right- and the left-hand branch points $z=\pm\rho=\pm(1+t_0/2k_s^2)$, [see Fig. 28(a)]; (2) f is bounded by s^N in D, where N is independent of s and z; (3) $\ln|f(s\ 1)|=O(\alpha, \ln s)$ with $\alpha<N$.

It turns out in the Cerulus and Martin result that $C(\theta)\to\infty$ at $z=0$. But we observe that one can obtain a finite lower bound which includes the point $z=0$ if one assumes that the lower bound for the function $f^{(t)}(s, t)$ is the same as that for $f(s, t)$ for $\theta\leq\pi/2$ (Chiu and Tan, 1967). Here $f^{(t)}$ is defined as follows:

$$f(s, t)\equiv f^{(t)}(s, t)+f^{(u)}(s, t), \tag{A2}$$

$$f^{(t)}(s, t)=\frac{1}{\pi}\int_{t_0}^{\infty}\frac{D_t(s, t')}{t'-t}\,dt', \tag{A2a}$$

and

$$f^{(u)}(s, t)=\frac{1}{\pi}\int_{u_0}^{\infty}\frac{D_u(s, u')}{u'-u}\,du'. \tag{A2b}$$

For simplicity, we have ignored subtractions in Eqs. (A2a) and (A2b). Note that the function $f^{(t)}$ now has only one cut, and a domain D' of boundedness and analyticity comparable to D is assumed [see Fig. 28(b)]. In general, one can choose the domain D' to be confined within some cone $A'AA''$ [see Fig. 28(c)], with its boundary tangential to the lines $A'A$ and and AA'', and $\angle CAA'=\angle CAA''=\theta$. Then, the generalized Cerulus–Martin lower bound is given by

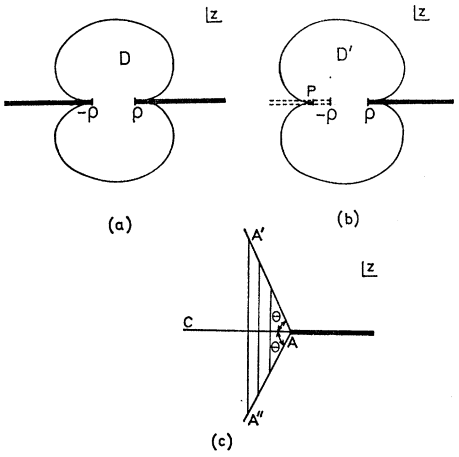

FIG. 28. (a) A schematic sketch of the domain D, where the analyticity and boundedness are assumed for the amplitude f, in the z plane. The boundaries of D are tangential to the real axis at the branch points $z=\pm\rho=\pm(1+t_0/2k_s^2)$. (b) A schematic sketch of the domain D', where analyticity and boundedness are assumed for the function $f^{(t)}$ in the z plane. The boundaries of D are tangential to the real axis at ρ and the point P, where P is some point along the real axis and $z_P<-\rho$. The dotted line indicates the left-hand cut which is absent for $f^{(t)}$. (c) The cut plane of $f^{(t)}$. The domain D' discussed in Appendix A.1 is chosen to be confined within the cone $A''AA'$.

$$f_{\mathrm{LB}}(s, \cos\theta_s)\xrightarrow[s\to\infty]{\text{fixed }\theta_s}\exp[-C_\gamma(\theta_s)s^\gamma\ln s], \tag{A3}$$

where $\gamma=\pi/2\theta$. For the result of (A1), the angle $\theta=\pi$. It can be shown for a linearly rising trajectory, that $\theta=\pi/2$, and thus $\gamma=1$. We refer the reader to the work of Chiu and Tan (1967), Eden and Tan (1968), and Epstein (1968) for further discussions concerning the generalization of the fixed-angle lower bound.

2. The Tiktopoulos–Treiman Asymptotic Angular Dependence

In Sec. 2.D we mentioned that a special significance of the $\sin\theta_s$ dependence in the Orear formula (1964) had recently been discussed by Tiktopoulos and Treiman (1968). We outline their assumptions and one of the methods for deducing this $\sin\theta_s$ dependence.* We refer the reader to the original paper for further details and their general results on various angular constraints.

Let $f(s, z)$ be the spin-averaged differential cross section. We are interested in the asymptotic angular dependence of f in the physical region $-1<z<1$. The assumptions made on $f(s, z)$ are as follows:

(1) $f(s, z)$ is analytic in some domain D_R in the z plane with cuts $[\rho, \infty]$ and $[-\rho, -\infty]$. For simplicity we shall only discuss the case for $R=1$ for which the domain $D_R\equiv D_1$ corresponds to the full cut plane. The possibility of weakening this condition was considered in the original paper.

(2) $|f(s, z)|\ll e^{Q(s)}|1+(\rho^2-z^2)^{1/2}|^{M(s)}$ for any z in D_1. Where the symbol "$\ll$" denotes the asymptotic inequality, i.e., if $x\ll y$, then

$$x/y\xrightarrow[s\to\infty]{}0.$$

(3) $f(s, z)$ has no zero in D_1.

Define

$$G(s, z)=-\ln f(s, z)+Q(s)+M(s)\ln[1+(\rho^2-z^2)^{1/2}].$$

From assumption (2), as $s\to\infty$,

$$\mathrm{Re}\,G(s, z)=-\ln|f(s, z)|+Q(s)+M(s)\ln|1+(\rho^2-z^2)^{1/2}|>0. \tag{A4}$$

To proceed further, one maps the domain D onto a unit circle, using the transformation

$$\omega=[(\rho+z)^{1/2}-(\rho-z)^{1/2}]/[(\rho+z)^{1/2}+(\rho-z)^{1/2}]. \tag{A5}$$

* The author would like to thank Professor R. E. Cutkosky for helpful discussions on this $\sin\theta_s$ dependence.

It can be shown that $\mathrm{Re}\,G(s,z)$ satisfies the following Poisson integral representation:

$$\mathrm{Re}\,G(s,z)=\frac{1}{2\pi}\int_{-\pi}^{\pi}\frac{1-\omega^2}{1-2\omega\cos\phi+\omega^2}\times\{\mathrm{Re}\,G[s,z'(e^{i\phi'})]\}d\phi'\equiv I(-\pi,\pi). \quad \text{(A6)}$$

For $s\to\infty$ and $-1<z<1$, for $\phi(s,z)=\ln|f(s,z)|$, we have

$$\phi(s,z)\approx\mathrm{Re}\,G(s,z)\equiv I_1+I_2, \quad \text{(A7)}$$

where

$$I_1=I(-\tfrac{1}{2}\pi-\epsilon,-\tfrac{1}{2}\pi+\epsilon)+I(\tfrac{1}{2}\pi-\epsilon,\tfrac{1}{2}\pi+\epsilon)$$

and

$$I_2=I(\tfrac{1}{2}\pi+\epsilon,-\tfrac{1}{2}\pi-\epsilon)+I(-\tfrac{1}{2}\pi+\epsilon,\tfrac{1}{2}\pi-\epsilon),\quad \text{with } \epsilon\ll 1. \quad \text{(A8)}$$

Then one assumes that $f(s,z_1)\ll f(s,z_2)$ for any z_1, z_2, where $-1<z_1<1$ and $z_2<-\rho$ or $z_2>\rho$. This, together with assumption (2) and Eq. (A8), implies that

$$\mathrm{Re}\,G(s,z)\gg I_2. \quad \text{(A9)}$$

Finally, from Eqs. (A7) and (A9), one obtains

$$\phi(s,z)\approx I_1=[(1-\omega^2)/(1+\omega^2)]g(s)=\sin\theta_s g(s), \quad \text{(A10)}$$

where

$$g(s)=\frac{1}{2\pi}\left\{\int_{-\pi/2-\epsilon}^{-\pi/2+\epsilon}\mathrm{Re}\,G[s,z'(e^{i\phi'})]d\phi'+\int_{\pi/2-\epsilon}^{\pi/2+\epsilon}\mathrm{Re}\,G[s,z'(e^{i\phi'})]d\phi'\right\}.$$

It turns out that Eq. (A10) is still valid even when there are zeros in the z plane, provided that

$$\frac{N(s)}{\phi(s,z)}\xrightarrow[s\to\infty]{}0,\quad \text{where } -1<z<+1, \quad \text{(A11)}$$

and $N(s)$ is the total number of zeros present in the z plane at fixed s.

APPENDIX B: MULTI-POMERANCHON EXCHANGE IN THE EIKONAL APPROXIMATION

We discuss here the behavior of the full multiple-scattering amplitude (Frautschi and Margolis, 1968a) when the Born amplitude, or the single-scattering amplitude, is given by

$$f_B/s^{1/2}=iC\exp(at). \quad \text{(B1)}$$

From Eq. (3.4) we have

$$\frac{f}{s^{1/2}}=iC\sum_{n=1}^{\infty}\frac{(-d)^{n-1}\exp(at/n)}{n\cdot n!}, \quad \text{(B2)}$$

where

$$d=C/2a.$$

For sufficiently large value of $|at|$, using the saddle-point method, one arrives at

$$f\sim\exp[-(-at\ln\bar{n})^{1/2}],\quad \text{where } \bar{n}=(-at/\ln\bar{n})^{1/2}. \quad \text{(B3)}$$

If the single-scattering term corresponds to single Pomeranchon exchange (let $\alpha_p=1+\alpha' t$ and assume in general that $\alpha'\neq 0$), then

$$f_B/s^{1/2}=Cs^{\alpha-1}\exp[i\pi(1-\alpha/2)]. \quad \text{(B4)}$$

The leading branch point associated with n-Pomeran-

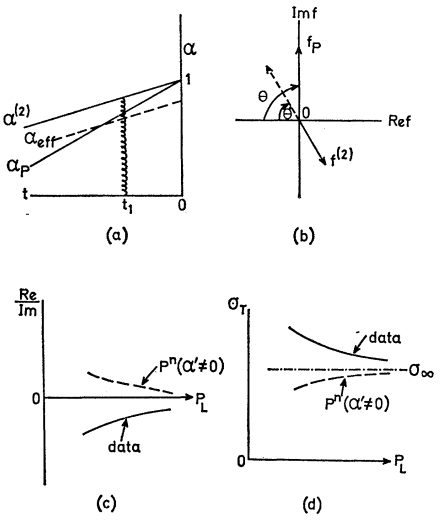

FIG. 29. (a) The plot of α versus t, where α_P, $\alpha^{(2)}$, and α_{eff} are, respectively, the Pomeranchon trajectory, the branch point of PP cut, and the effective α for the phase of PP cut contribution at a given energy. (b) The Argand diagram for f_p and $f^{(2)}$, where f_p is the single Pomeranchon amplitude and $f^{(2)}$ is the double Pomeranchon cut amplitude. Note that $\theta=\pi\alpha_p/2$ and $\theta'=\pi\alpha^{(2)}/2$. (c) The ratio of real part to imaginary part of the forward amplitude versus P_L. The solid line indicates the behavior of the data, and the dotted line the contribution from multi-Pomeranchon exchange with $\alpha_p'\neq 0$. (d) The total cross section versus P_L. The solid line indicates the behavior of the data. The dash-dot line indicates the asymptotic total cross section, and the dashed line the contribution due to multi-Pomeranchon exchange with $\alpha_P'\neq 0$.

chon exchange is given by

$$\alpha^{(n)}=1+\alpha' t/n. \tag{B5}$$

One can easily check that the $1/n$ factor in Eq. (B5) is closely related to that in the exponent in Eq. (B2). At this stage it is instructive to look at the phase associated with the Pomeranchon and the Pomeranchon cuts. Since at $t=0$ in the asymptotic limit, the two Pomeranchon cut is the leading cut, we shall consider only the single- and the double-scattering terms. In Fig. 29(a) we plot α_p and $\alpha^{(2)}$. At any fixed momentum transfer, the cut contribution corresponds to the exchange of a continuum of the angular momentum with its maximum at $\alpha^{(2)}(t_1)$. At a given energy, there is an effective angular momentum characterizing the resultant phase associated with the cut contribution. We denote this effective angular momentum by the dotted line. The phases of the P pole and the PP cut are illustrated in Fig. 29(b). At $t=0$, P is purely imaginary and the PP cut is in the fourth quadrant; there is an extra minus sign associated with the eikonal expansion [see Eq. (4.4)]. From Fig. 29(b) one can easily see that, due to muli-Pomeranchon exchange, one expects the ratio of real part to imaginary part of the forward-scattering amplitude to approach zero from the positive side [see Fig. 29(c)] and σ_T to approach $\sigma_T(\infty)$ from below [see Fig. 29(d)]. These two features are in contradiction to the presently observed behavior. These points have been noticed by Finkelstein and the author (1968a) and recently emphasized by Frautschi and Margolic (1968a; 1968b). There are three possible factors which can help to correct this behavior:

(1) $\alpha_p'\approx 0$, as suggested by Chou–Yang model; it is used explicitly in the hybrid model.

(2) α_p has a nominal slope; at present energies the secondary trajectory contribution masks the effects of the cut. As emphasized by Frautschi and Margolis, we expect to see these features only at extreme asymptotic energies.

(3) α_p has a nominal slope, but the alternating sign prescription for the cuts is incorrect. We feel this last possibility is unlikely in view of the experimental evidences favoring this sign alteration. We mention the following evidence: (a) the existence of the diffraction pattern; (b) the cross-over effect; and (c) the sign of the $\pi^- p\to\pi^0 n$ polarization (Finkelstein and Jacob, 1968).

ACKNOWLEDGMENTS

I would like to thank my colleague Dr. J. Finkelstein for his critical remarks on this paper. This manuscript was prepared during my visit to the Cavendish Laboratory. I wish to express my appreciation to Dr. R. J. Eden for helpful discussions and to thank Clare Hall for a Visiting Fellowship. A summary of this paper was presented at the Rutherford Laboratory Theoretical Physics Meeting, December 1968. I would like to thank Dr. R. J. N. Phillips and Dr. G. C. Oades for their kind invitation of the talk. I wish to acknowledge that I have benefited from discussions with Professor R. E. Cutkosky and Professor J. Polkinghorne. Finally, I must thank Dr. A. Wetherell for forwarding me some original drawings, and thanks to Dr. J. J. Kubis, and Mr. R. L. Heimann for their help in bringing the article to the final form.

REFERENCES

J. V. Allaby *et al.*, *Proceedings of Topical Conference on High Energy Collisions of Hadrons* (CERN, Geneva, 1968a), p. 580.
J. V. Allaby, F. Binon, A. N. Diddens, P. Duteil, A Klovning, R. Meunier, J. P. Peigneux, E. J. Sacharidis, K. Schlüpmann, M. Spighel, J. P. Stroot, A. M. Thorndike, and A. M. Wetherell, Phys. Letters **28B**, 67 (1968b).
J. V. Allaby, F. Binon, A. N. Diddens, P. Duteil, A. Klovning, R. Meunier, J. P. Peigneux, E. J. Sarcharidis, K. Schlüpmann, M. Spighel, J. P. Stroot, A. M. Throndike, and A. M. Wetherell, Phys. Letters **28B**, 229 (1968c).
J. V. Allaby, G. Cocconi, A. N. Diddens, A. Klovning, G. Matthiae, E. J. Sacharidis and A. M. Wetherell, Phys. Letters **25B**, 156 (1967).
J. V. Allaby, G. Bellettini, G. Cocconi, A. N. Diddens, M. L. Good, G. Matthiae, E. J. Sacharidis, A. Silverman and A. M. Wetherell, Phys. Letters **23**, 389 (1966).
D. Amati, M. Cini, and A. Stanghellini, Nuovo Cimento **30**, 193 (1963).
A. A. Anselm and I. T. Dyatlov, Phys. Letters **24B**, 479 (1967a).
A. A. Anselm and I. T. Dyatlov, Yadern. Phys. **6**, 591 (1967b).
A. A. Anselm and I. T. Dyatlov, Yadern. Phys. **6**, 603 (1967c).
F. Arbab, N. F. Bali, and J. W. Dash, Phys. Rev. **158**, 1515 (1967).
F. Arbab and C. B. Chiu, Phys. Rev. **147**, 1045 (1966).
H. D. I. Arbarbanel, S. D. Drell, and F. Gilman, Phys. Rev. Letters **20**, 280 (1968a).
H. D. I. Arbarbanel, S. D. Drell and F. Gilman, "The Structure of High-Energy Proton–Proton Scattering," a paper contributed to the XIVth International Conference on High Energy Physics, Vienna, 1968b.
R. C. Arnold, The Next Step in High Energy Phenomenology," Argonne National Laboratory Preprint, 1968.
R. C. Arnold, Phys. Rev. **153**, 1523 (1967).
R. C. Arnold and M. L. Blackmon, Regge-Pole Eikonal Theory of Small-Angle Pion–Nucleon Scattering," a paper submitted to the XIVth International Conference on High Energy Physics, Vienna, 1968.
J. G. Asbury, L. G. Ratner, A. L. Read, D. G. Crabb, J. L. Day, A. D. Krisch, M. T. Lin, and M. L. Marshak, Phys. Rev. Letters **21**, 1097 (1968).
A. Ashmore, C. J. S. Damerell, W. R. Frisken, R. Rubinstein, J. Orear, D. P. Owen, F. C. Peterson, A. L. Read, D. G. Ryan, and D. H. White, Phys. Rev. Letters **21**, 387 (1968).
V. Barger, in *Proceedings of Topical Conference on High Energy Collisions of Hadrons* (CERN, Geneva, 1968).
V. Barger and D. Cline, Phys. Rev. Letters **21**, 392 (1968).
V. Barger and R. J. N. Phillips, Phys. Rev. Letters **22**, 116 (1969).
V. Barger and R. J. N. Phillips, Phys. Rev. Letters **20**, 564 (1968).
G. Bellettini, Rapporteur's talk, in Proceedings of the XIVth International Conference on High Energy Physics, Vienna, 1968.
A. Beretvas and N. E. Booth, Phys. Rev. Letters **22**, 113 (1969)
D. Birnbaum *et al.*, Proceedings of the XIVth Internationa Conference on High Energy Physics, Vienna, 1968, Paper 719.
R. Blankenbecler and M. L. Goldberger, Phys. Rev. **126**, 766 (1962).
K. Böckmann, B. Nellen, E. Paul, B. Wagini, I. Borecka, J. Diaz, U. Heeren, U. Liebermeister, E. Lohrmann, E. Raubold, P. Söding, S. Wolff, J. Kidd, L. Mandell, L. Mosca, V. Pelosi, S. Ratti, and L. Tallone, Nuovo Cimento **42A**, 954 (1966).

N. E. Booth, Phys. Rev. Letters **21,** 465 (1968).
N. Byers and C. N. Yang, Phys. Rev. **142,** 976 (1966).
F. Cerulus and A. Martin, Phys. Letters **8,** 80 (1964).
H.-M. Chan, Review paper presented at the XIVth International Conference on High Energy Physics, Vienna, 1968.
C. B. Chiu, S. Y. Chu, and L. L. Wang, Phys. Rev. **161,** 1563 (1967).
C. B. Chiu and J. Finkelstein, Nuovo Cimento **57A,** 649 (1968a).
C. B. Chiu and J. Finkelstein, Phys. Letters **27B,** 510 (1968b).
C. B. Chiu and J. Finkelstein, Nuovo Cimento **59A,** 92 (1969).
C. B. Chiu and J. D. Stack, Phys. Rev. **153,** 1575 (1967).
C. B. Chiu and C. I. Tan, Phys. Rev. **162,** 1701 (1967).
T. T. Chou and C. N. Yang, Phys. Rev. **170,** 1591 (1968a).
T. T. Chou and C. N. Yang, Phys. Rev. Letters **20,** 1213 (1968b).
A. R. Clyde, UCRL-16275 (1966).
G. Cocconi, V. T. Cocconi, A. D. Krisch, J. Orear, R. Rubinstein, D. B. Scarl, B. T. Ulrich, W. F. Baker, E. W. Jenkins, and A. L. Read, Phys. Rev. **138,** B165 (1965).
C. T. Coffin, N. Dikmen, L. Ettlinger, D. Meyer, A. Saulys, K. Terwilliger, and D. Williams, Phys. Rev. Letters **17,** 458 (1966).
C. T. Coffin, N. Dikmen, L. Ettlinger, D. Meyer, A. Saulys, K. Terwilliger and D. Williams, Phys. Rev. Letters **15,** 838 (1965).
G. Cohen-Tannoudji A. Morel, and H. Navelet, Nuovo Cimento **48,** 1075 (1967).
A. P. Contogouris Phys. Letters **23,** 698 (1966).
L. Durand III and R. Lipes, Phys. Rev. Letters **20,** 637 (1968).
R. J. Eden and C. I. Tan, Phys. Rev. **172,** 1583 (1968).
H. Epstein, in *Proceedings of Topical Conference on High Energy Collisions of Hadrons* (CERN, Geneva, 1968), p. 290.
J. E. O. Ericson, *Lectures in Theoretical Physics,* P. D. Kunz, D. A. Lind, and W. E. Brittin, Eds. (University of Colorado Press, Boulder, Colorado, 1966), Vol. 8C, p. 299.
G. Fast and R. Hagedorn, Nuovo Cimento **27,** 203 (1963).
G. Fast, R. Hagedorn and L. W. Jones, Nuovo Cimento **27,** 856 (1963).
J. Finkelstein and M. Jacob, Nuovo Cimento **56,** 681 (1968).
K. J. Foley, R. S. Jones, S. J. Lindenbaum, W. A. Love, S. Ozaki, E. D. Platner, C. A. Quarles, and E. H. Willen, Phys. Rev. Letters **19,** 857 (1967).
K. J. Foley, R. S. Gilmore, S. J. Lindenbaum, W. A. Love, S. Ozaki, E. H. Willen, R. Yamada, and L. C. L. Yuan, Phys. Rev. Letters **15,** 45 (1965).
K. J. Foley, S. J. Lindenbaum, W. A. Love, S. Ozaki, J. J. Russell and L. C. L. Yuan, Phys. Rev. Letters **11,** 425 (1963a).
K. J. Foley, S. J. Lindenbaum, W. A. Love, S. Ozaki, J. J. Russell, and L. C. L. Yuan, Phys. Rev. Letters **11,** 503 (1963b).
S. Frautschi and B. Margolis, "Multiple Scattering Corrections to Pomeron Exchange," CERN Preprint, 909 (1968a).
S. Frautschi and B. Margolis, "Multiple Scattering and Isobar Production," CERN Preprint, 916 (1968b).
P. G. O. Freund, Phys. Rev. Letters **20,** 235 (1968).
R. J. Glauber, *High Energy Physics and Nuclear Structure,* (North-Holland Publ. Co., Amsterdam, 1967), p. 311.
R. J. Glauber, *Lectures in Theoretical Physics* (Interscience Publishers, Inc., New York, 1959), Vol. I, p. 315.
V. N. Gribov, Sov. Phys.—JETP **26,** 414 (1968).
V. N. Gribov, I. Ya. Pomeranchuk, and K. A. Ter-Martirosyan, Phys. Rev. **139,** B184 (1965).
H. Harari, Phys. Rev. Letters **20,** 1395 (1968).
D. Harrington and A. Pagnamenta, Phys. Rev. **173,** 1599 (1968).
F. Henyey, G. L. Kane, J. Pumplin, and M. Ross, Phys. Rev. Letters **21,** 946 (1968).
G. Höhler, H. Schaile, and P. Sonderegger, Phys. Letters **20,** 79 (1966).
I. Kimel and H. Miyazawa, "Absorption Hard Core and Regge Cuts," University of Chicago Preprint, 1967.
J. J. J. Kokkedee and L. Van Hove, Phys. Letters **25B,** 228 (1967).
M. N. Kreisler, F. Martin, M. N. Perl, M. J. Longo, and S. T. Powell III, Phys. Rev. Letters **16,** 1217 (1966).
A. D. Krisch, *Lectures in Theoretical Physics,* W. E. Brittin and A. O. Barut, Eds. (University of Colorado Press, Boulder, Colorado, 1967a), Vol. 9B, p. 1.
A. D. Krisch, Phys. Rev. Letters **19,** 1149 (1967b).
S. Mandelstam, Nuovo Cimento **30,** 1148 (1963).
G. Manning, A. G. Parham, J. D. Jafar, H. B. van der Raay, D. H. Reading, D. G. Ryan, B. D. Jones, J. Malos, and N. H. Lipman, Nuovo Cimento **41,** 167 (1966).
J. Mott, R. Ammar, R. Davis, W. Dropac, A. Cooper, M. Derrick, T. Fields, L. Hyman, J. Loken, F. Schweingruber, and J. Simpson, Phys. Letters **23,** 171 (1966).
J. Orear, D. P. Owen, F. C. Peterson, A. L. Read, D. G. Ryan, D. H. White, A. Ashmore, C. J. S. Damerell, W. R. Frisken, and R. Rubinstein, Phys. Letters **28B,** 61 (1968a).
J. Orear, D. P. Owen, F. C. Peterson, A. L. Read, D. G. Ryan D. H. White, A. Ashmore, C. J. S. Damerell, W. R. Frisken, and R. Rubenstein, Phys. Rev. Letters **21,** 389 (1968b).
J. Orear, R. Rubinstein, D. B. Scarl, D. H. White, A. D. Krisch, W. R. Frisken, A. L. Read, and H. Ruderman, Phys. Rev. **152,** 1162 (1966).
J. Orear, Phys. Letters **13,** 190 (1964).
R. J. N. Phillips and W. Rarita, Phys. Letters **19,** 598 (1965a).
R. J. N. Phillips and W. Rarita, Phys. Rev. **139,** B1336 (1965b).
J. C. Polkinghorne, Nuovo Cimento **56A,** 755 (1968a).
J. C. Polkinghorne, Nucl. Phys. **B6,** 441 (1968b).
J. C. Polkinghorne, J. Math. Phys. **6,** 1960 (1965).
J. C. Polkinghorne, J. Math. Phys. **4,** 1396 (1963).
R. Rivers, Nuovo Cimento **57A,** 174 (1968).
E. J. Squires, Phys. Letters **26B,** 461 (1968).
G. Tiktopoulos and S. B. Treiman, Phys. Rev. **167,** 1437 (1968).
L. Van Hove, *Proceedings of the Conference on High-Energy Two-Body Reactions* (Stony Brook, New York, 1966).
C. Wilkin, in *Nuclear and Particle Physics,* B. Margolis and C. S. Lam, Eds. (W. A. Benjamin, Inc., New York, 1968), p. 439.
T. T. Wu and C. N. Yang, Phys. Rev. **137,** B708 (1965).